INTERNATIONAL JOURNAL FOR NUMERICAL AND ANALYTICAL METHODS IN GEOMECHANICS

Int. J. Numer. Anal. Meth. Geomech. 2005; **01**:1 *Prepared using* nagauth.cls *[Version: 2000/03/22 v1.0]*

Directional response of a reconstituted fine–grained soil. Part II: Performance of different constitutive models

David Mašín[1,*], Claudio Tamagnini[2]

Gioacchino Viggiani[3], Daniele Costanzo[4]

[1] *Charles University, Prague, Czech Republic*

[2] *Università degli Studi di Perugia, Perugia, Italy*

[3] *Laboratoire 3S, UJF – INPG – CNRS, Grenoble, France*

[4] *Politecnico di Torino, Torino, Italy*

SUMMARY

In this paper, the performance of different advanced constitutive models for soils is evaluated with respect to the experimentally observed behavior of a soft reconstituted clay subject to a wide range of loading directions, see Costanzo et al. (2006). The models considered include a three–surface kinematic hardening elastoplastic model (Stallebrass, 1990); the CLoE hypoplastic model (Chambon et al., 1994); a recently proposed K–hypoplastic model for clays (Mašín, 2005), and an enhanced version of the same model incorporating the concept of intergranular strain. A clear qualitative picture of the relative performance of the different models as a function of the loading direction is obtained by means of the incremental strain response envelopes. The definition of suitable error measures allows to

*Correspondence to: David Mašín, Institute of Hydrogeology, Engineering Geology and Applied Geophysics, Charles University, Albertov 6, 128 43 Prague 2, Czech Republic

obtain further quantitative information in this respect. For the particular initial conditions and loading programme considered in this study, the kinematic hardening and the enhanced K-hypoplastic models appear to provide the best performance overall.

KEY WORDS: Incremental non–linearity, plasticity, hypoplasticity, strain response envelopes.

1. INTRODUCTION

The directional character of the mechanical response of fine–grained soils, i.e., its dependence on the loading direction, has been the subject of several studies throughout the last decades, including both experimental and theoretical investigations. On the experimental side, some pioneering contributions were provided in the early seventies, see e.g., Lewin and Burland (1970), Wood (1974). Notable examples of more recent contributions can be found in the works of Graham et al. (1983), Atkinson et al. (1990), Smith et al. (1992) and Callisto and Calabresi (1998). On the theoretical side, a major improvement of classical plasticity as applied to clays has been provided by the introduction of the so–called nested–surface kinematic hardening theories of plasticity, originating from the works of Prevost (1977), Mroz et al. (1978) and Hashiguchi (1985). These latter studies were essentially motivated by the need of improving available design approaches for those practical applications where soil is subject to cyclic loading conditions, e.g., earthquakes, offshore engineering, etc.

Later studies on shear banding in soils as a bifurcation problem (Rudnicki and Rice, 1975; Rice, 1976) showed the need to take into account the *incrementally non–linear* character of the material response – i.e., a dependence of soil tangent stiffness on the strain rate direction,

see, e.g., Darve (1990), Tamagnini and Viggiani (2002) – and motivated the development of a class of constitutive theories which depart from the framework of plasticity and rather can be seen as a generalization of Truesdell theory of hypoelasticity (Truesdell, 1956). A distinctive feature of this approach is the absence of any kinematic decomposition of strain rates into reversible and irreversible parts. An important example in this respect is provided by the theory of hypoplasticity, as defined by Kolymbas (1991), see also Lanier et al. (2004).

More generally, it turns out that a proper description of soil behavior as a function of loading direction not only is useful for modelling the response of geotechnical structures to cyclic loading or for analyzing localization phenomena, but it is also a key ingredient in the analysis of any geotechnical structure where different zones of soil experience widely different stress–paths, both in size and direction, e.g., deep excavations and tunnels. This has been demonstrated in a number of practical applications, see, e.g. St. John et al. (1993), Whittle et al. (1993), Finno et al. (1989), Viggiani and Tamagnini (2000).

The objective of this work is to assess, both qualitatively and quantitatively, the performance of some advanced constitutive models in reproducing the stress–strain behavior of a soft, normally consolidated reconstituted clay as observed in laboratory tests performed along a number of different stress–paths originating from a common initial state. Two particular classes of inelastic models have been selected for the comparison. On the one hand, the three–surface kinematic hardening model proposed by Stallebrass (1990); Stallebrass and Taylor (1997) has been chosen as the representative candidate of modern soil plasticity approaches. On the other hand, three different versions of hypoplasticity have been considered, which differ from each other in terms of history–related state variables, namely the CLoE model (Chambon et al., 1994), the clay K–hypoplastic model recently proposed by Mašín (2005), and a modified version

of this last model, embedding the concept of intergranular strain (Niemunis and Herle, 1997) as additional internal state variable. Finally, the classical critical–state Modified Cam–Clay model with associative flow rule (Roscoe and Burland, 1968) has been also considered as a reference.

The companion paper by Costanzo et al. (2006) presents the results of a large program of stress–probing tests on normally consolidated, reconstituted Beaucaire Marl. These results are used herein both for the calibration of the different models, and as a benchmark for the evaluation of the models performance. The results obtained from standard isotropic or triaxial compression and extension tests, starting from an isotropic state, were used for the calibration of the different models. The assessment of models' performance was carried out with reference to a different set of data, obtained from axisymmetric stress–probing tests starting from an anisotropic initial stress state.

The outline of the paper is as follows. The details of the experimental program are shortly recalled in Sect. 2. A summary of the main features of the constitutive models considered is provided in Sect. 3. The procedures adopted for the calibration of the different models are thoroughly discussed in Sect. 4, before presenting the comparison between predicted and observed directional response, in Sect. 5, where a quantitative assessment of the performance of the models is attempted by introducing suitable scalar measures of the prediction error. Finally, some concluding remarks are drawn and perspectives for further research are provided in Sect. 6.

In the following, the usual sign convention of soil mechanics (compression positive) is adopted throughout. In line with Terzaghi's principle of effective stress, all stresses are *effective* stresses, unless otherwise stated. Both direct and index notation will be used to represent

tensor quantities, according to convenience. Calligraphic letters are used to represent fourth–order tensors and their components (e.g., $\boldsymbol{\mathcal{L}}$ and $\mathcal{L}_{ijkl}$). In the representation of stress and strain states, use is sometimes made of the following invariant quantities: $p := (1/3)\,\mathrm{tr}\,\boldsymbol{\sigma}$ (mean stress); $q := \sqrt{(3/2)}\,\|\mathrm{dev}(\boldsymbol{\sigma})\|$ (deviatoric stress); $\epsilon_v := \mathrm{tr}\,\boldsymbol{\epsilon}$ (volumetric strain); and $\epsilon_s := \sqrt{(2/3)}\,\|\mathrm{dev}(\boldsymbol{\epsilon})\|$ (deviatoric stress).

2. EXPERIMENTAL DATA FROM STRESS–PROBING TESTS

The material tested is a low plasticity silty clay, with a liquid limit of 38%, and a plasticity index of 17%. The stress–probing tests were performed on reconstituted material, consolidated in a large consolidometer up to a nominal vertical effective stress of 75 kPa. Full details of the experimental procedures employed in the testing program are given by Costanzo et al. (2006). Overall, the measurement system is capable of resolving strains of approximately 0.0005.

The testing program consisted of a large number of drained stress probes, starting from a common initial stress state and pointing in different directions in the triaxial plane. Two different initial stress states were considered: the first one (state A) is located on the isotropic axis at $p = 150$ kPa; the second one (state B) is characterized by the same mean stress as state A and a deviator stress $q = 60$ kPa. Both states A and B were reached upon stress–controlled consolidation along a constant q/p path ($q/p = 0$ for state A, $q/p = 0.4$ for state B). Each stress probe from an initial state $(\sigma_{a0}, \sigma_{r0})$ is described by the following parametric equations:

$$\Delta\sigma_a := \sigma_a - \sigma_{a0} = R_\sigma \sin\alpha_\sigma \tag{2.1}$$

$$\sqrt{2}\,\Delta\sigma_r := \sqrt{2}\,\sigma_r - \sigma_{r0} = R_\sigma \cos\alpha_\sigma \tag{2.2}$$

where $R_\sigma = \|\Delta\boldsymbol{\sigma}\|$ denotes the norm of the stress increment, and α_σ represents its direction

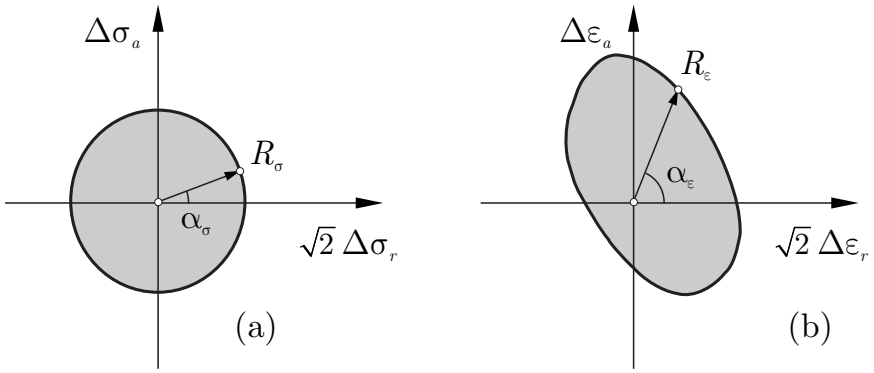

Figure 1. Response envelope concept: a) input stress probes; b) output strain envelope.

in the Rendulic plane of stress increments ($\Delta\sigma_a : \sqrt{2}\,\Delta\sigma_r$, see Fig. 1a). Each stress probe was continued up to a R_σ value corresponding either to a "failure" state, or to a prescribed maximum value of the cell pressure. The loading directions α_σ prescribed for each probe are listed in Tab. I. Note that for each initial state the testing program included as particular cases conventional triaxial, constant p and isotropic, compression and extension paths. The stress probe direction in the $q : p$ plane, α_σ^{pq}, calculated from the stress invariant increments $\Delta\, p$ and $\Delta\, q$ as:

$$\Delta\, p = \frac{1}{3}\left(\Delta\sigma_a + 2\Delta\sigma_r\right) \qquad \Delta\, q = \Delta\sigma_a - \Delta\sigma_r \tag{2.3}$$

$$\sin\alpha_\sigma^{pq} = \frac{\Delta\, q}{\sqrt{(\Delta\, p)^2 + (\Delta\, q)^2}} \qquad \cos\alpha_\sigma^{pq} = \frac{\Delta\, p}{\sqrt{(\Delta\, p)^2 + (\Delta\, q)^2}} \tag{2.4}$$

is also reported in the same table. A picture of the stress paths originating from initial state B in the $q : p$ plane is shown in Fig. 2.

Test #	Initial state	α_σ (deg.)	α_σ^{pq} (deg.)	Test #	Initial state	α_σ (deg.)	α_σ^{pq} (deg.)
Tx124	A	0	303.69	Tx118	B	0	303.69
Tx128	A	35	0.00	Tx115	B	35	0.00
—	—	—	—	Tx130	B	46	21.91
Tx121	A	90	71.57	Tx132	B	90	71.57
Tx126	A	126	90.00	Tx119	B	126	90.00
—	—	—	—	Tx116	B	154	104.49
Tx123	A	180	123.69	—	—	—	—
Tx127	A	215	180.00	Tx134	B	215	180.00
—	—	—	—	Tx129	B	226	201.91
Tx122	A	270	251.57	Tx117	B	270	251.57
Tx125	A	305	270.00	Tx113	B	305	270.00

Table I. Details of the experimental stress–probing program, after Costanzo et al. (2006).

3. CONSTITUTIVE MODELS CONSIDERED

3.1. The 3–SKH model

The 3–SKH model is an advanced example of the kinematic hardening plasticity models originating from the pioneering work of Prevost (1977); Mroz et al. (1978). The model is based on the principles of critical state soil mechanics and represents an evolution of the classical Modified Cam–Clay model (Roscoe and Burland, 1968), and the two–surface kinematic hardening model proposed by Al Tabbaa and Wood (1989). The main feature of

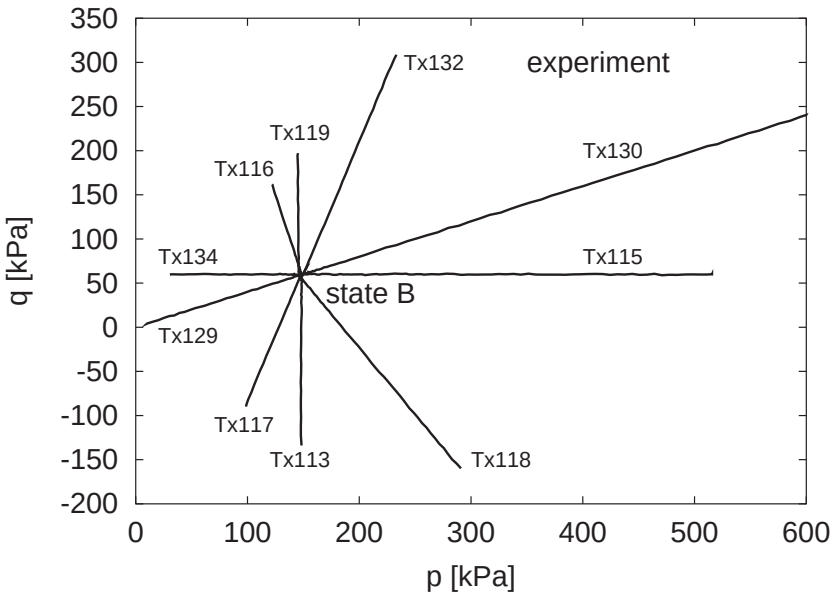

Figure 2. Experimental stress–probes performed from state B

the 3–SKH model consists in the introduction of an additional kinematic *history surface* – as defined in Stallebrass (1990), see Fig. 3 – motivated by experimental findings about the influence of the recent stress history on soil behavior (Atkinson et al., 1990). While kinematic hardening models are capable of dealing with cyclic loading conditions and, more generally, of reproducing the observed non–linear behavior inside the state boundary surface, 3–SKH model provides significantly improved predictions in the small strain range, see Stallebrass and Taylor (1997). Successful applications of this model at both the single–element level and in the analysis of typical boundary value problems are reported, *e.g.*, by Grant et al. (1996), Ingram (2000), Baudet (2001) and Mašín (2004). The general formulation of the 3–SKH model is given in Appendix B.

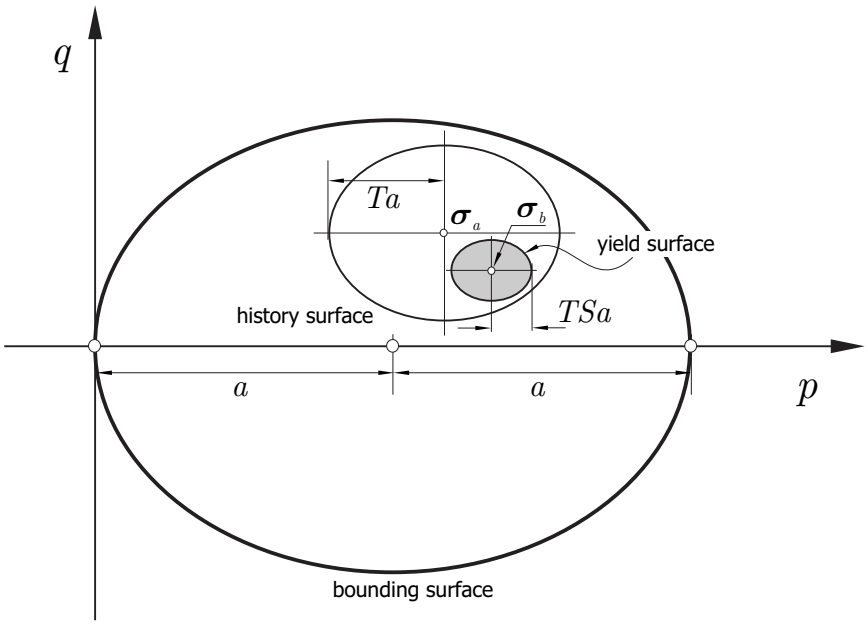

Figure 3. Sketch of the characteristic surfaces of the 3–SKH model

3.2. The CLoE hypoplastic model

The origins of CLoE hypoplasticity — where the acronym CLoE stands for *Consistance et Localisation Explicite* — can be traced back to the pioneering work of Chambon and Desrues on strain localization in incrementally non–linear materials Chambon and Desrues (1985); Desrues and Chambon (1989). The constitutive equation is given, in rate–form, by:

$$\dot{\boldsymbol{\sigma}} = \boldsymbol{\mathcal{A}}(\boldsymbol{\sigma})\dot{\boldsymbol{\epsilon}} + \boldsymbol{b}(\boldsymbol{\sigma})\ \|\dot{\boldsymbol{\epsilon}}\| \tag{3.1}$$

see (Chambon et al., 1994). The first term on the right–hand side yields an incrementally linear response, while the second accounts for incremental non–linearity via a linear dependence on the norm of the strain rate tensor. To keep the formulation as simple as possible, the set of state variables for the material is limited to the Cauchy stress tensor.

An essential feature of CLoE model is that the constitutive response in stress space is bounded by an explicitly assumed limit surface, separating admissible from impossible stress states. The particular form adopted for the limit surface is given by the equation proposed by van Eekelen (1980), which allows for different values of friction angle in compression and extension. When the stress state reaches the limit surface, it is explicitly assumed that no outer stress rate response can be generated by any applied strain rate (*consistency condition*).

The two constitutive tensors $\boldsymbol{\mathcal{A}}$ and $\boldsymbol{b}$ appearing in (3.1) are homogeneous functions of degree one of the stress tensor, for which no explicit expression is assumed. Rather, $\boldsymbol{\mathcal{A}}$ and $\boldsymbol{b}$ are obtained via an interpolation procedure based on the assigned material responses at some suitably defined image points, located along special loading paths (*basic paths*). These are selected among those stress–paths that are experimentally accessible by means of conventional laboratory tests. The consistency condition at limit states implies a series of additional requirements for the components of $\boldsymbol{\mathcal{A}}$ and $\boldsymbol{b}$, see Chambon et al. (1994). Details on the basic paths and on the constitutive functions employed to represent the stress–strain behavior of the soil along them will be given when detailing the calibration procedure.

3.3. The K–hypoplastic model for clays

The K–hypoplastic model considered in the present study has been recently developed by Mašín (2005) with the specific aim of describing the behavior of fine–grained soils. The model combines the mathematical structure of K–hypoplastic models – see *e.g.*, Wu and Kolymbas (2000) and references therein – with key concepts of critical state soil mechanics (Schofield and Wroth, 1968) through the notion of generalised hypoplasticity, as defined by Niemunis (2002). In fact, the model can be considered an evolution of both von Wolffersdorff (1996) model for

sands, and the more recent Herle and Kolymbas (2004) model for soils with low friction angles

The constitutive equation is given, in rate–form, by:

$$\dot{\boldsymbol{\sigma}} = f_s \boldsymbol{\mathcal{L}} : \dot{\boldsymbol{\epsilon}} + f_s f_d \boldsymbol{N} \|\dot{\boldsymbol{\epsilon}}\| \tag{3.2}$$

Explicit, closed form expressions for the two tensors $\boldsymbol{\mathcal{L}}(\boldsymbol{\sigma})$ and $\boldsymbol{N}(\boldsymbol{\sigma})$ and for the scalar functions $f_s(p)$ and $f_d(p, e)$ are provided in Appendix B. It must be noted that, although Eq. (3.2) and (3.1) appear quite similar, a major difference of K–hypoplasticity as compared to CLoE stems from including void ratio in the set of state variables for the material through the so–called *pyknotropy factor* f_d (Gudehus, 1996). It is precisely this ingredient which allows the critical state concept to be incorporated in the constitutive equation. A more general comparison between the two frameworks of CLoE– and K–hypoplasticity can be found in Tamagnini et al. (2000).

3.4. The K–hypoplastic model for clays with intergranular strain

The K–hypoplastic model discussed in the previous section is capable of predicting the behavior of fine–grained soils upon monotonic loading at medium to large strain levels. In order to prevent excessive ratcheting upon cyclic loading and to improve model performance in the small–strain range, its mathematical formulation has been enhanced by the intergranular strain concept (Niemunis and Herle, 1997).

The mathematical formulation of this enhanced version of the K–hypoplastic model for clays is given by:

$$\dot{\boldsymbol{\sigma}} = \boldsymbol{\mathcal{M}}\left(\boldsymbol{\sigma}, e, \boldsymbol{\delta}, \boldsymbol{\eta}\right) : \dot{\boldsymbol{\epsilon}} \tag{3.3}$$

where $\boldsymbol{\mathcal{M}}$ is the fourth–order tangent stiffness tensor of the material, $\boldsymbol{\eta} := \dot{\boldsymbol{\epsilon}} / \|\dot{\boldsymbol{\epsilon}}\|$ denotes the strain rate direction, and the additional state variable $\boldsymbol{\delta}$ is a symmetric second order tensor

called *intergranular strain*. Full details of the mathematical structure of the model are provided in appendix B.

In this formulation, the total strain can be thought of as the sum of a component related to the deformation of interface layers at integranular contacts, quantified by $\boldsymbol{\delta}$, and a component related to the rearrangement of the soil skeleton. For reverse loading conditions ($\boldsymbol{\eta} : \hat{\boldsymbol{\delta}} < 0$, where $\hat{\boldsymbol{\delta}}$ is defined in Appendix B) and neutral loading conditions ($\boldsymbol{\eta} : \hat{\boldsymbol{\delta}} = 0$), the observed overall strain is related only to the deformation of the intergranular interface layer and the soil behaviour is hypoelastic, whereas in continued loading conditions ($\boldsymbol{\eta} : \hat{\boldsymbol{\delta}} > 0$) the observed overall response is also affected by particle rearrangement in the soil skeleton. From a mathematical standpoint, the response of the model is determined by interpolating between the following three special cases:

$$\dot{\boldsymbol{\sigma}} = m_R f_s \boldsymbol{\mathcal{L}} : \dot{\boldsymbol{\epsilon}} \qquad (\boldsymbol{\eta} : \hat{\boldsymbol{\delta}} = -1 \ \wedge \ \boldsymbol{\delta} = 0) \tag{3.4}$$

$$\dot{\boldsymbol{\sigma}} = m_T f_s \boldsymbol{\mathcal{L}} : \dot{\boldsymbol{\epsilon}} \qquad (\boldsymbol{\eta} : \hat{\boldsymbol{\delta}} = 0) \tag{3.5}$$

$$\dot{\boldsymbol{\sigma}} = f_s \boldsymbol{\mathcal{L}} : \dot{\boldsymbol{\epsilon}} + f_s f_d \boldsymbol{N} \, \|\dot{\boldsymbol{\epsilon}}\| \qquad (\boldsymbol{\eta} : \hat{\boldsymbol{\delta}} = 1) \tag{3.6}$$

the last case corresponding to the so–called *swept–out–memory* conditions (Gudehus et al., 1977). The quantities m_R and m_T appearing in Eqs. 3.4 and 3.5 are material constants. The particular structure adopted for the constitutive tensor $\boldsymbol{\mathcal{L}}$ (Mašín, 2005) should allow, in principle, to get a good performance in both the very small and large strain ranges.

4. MODEL CALIBRATION

When comparing the performance of different constitutive models in predicting the observed directional response of the material, particular care must be taken in the proper selection of the

procedure adopted for their calibration. In the present case, this task is somewhat made easier by the fact that all the constitutive models discussed in the previous section, with the only exception of the CLoE hypoplastic model, incorporate the basic principles of Critical State Soil Mechanics, and thus some of the material constants share the same physical meaning.

In order to separate the data used for the calibration of the five models considered and the data used for the evaluation of their performance, the material constants of each model have been determined from the results of the stress probes starting from the isotropic initial state A. This is also consistent with the procedure typically used in practical applications, where most of the experimental data provided by the site investigation refer to isotropically consolidated, drained or undrained triaxial tests.

For some of the constitutive models considered, the available data from stress probes at point A do not provide enough information to calibrate all the relevant constants. This is the case, for example, of the material parameters controlling the response of the 3–SKH or K–hypoplastic models upon load reversal in the very small strain range. In such cases, the choice has been made to evaluate such material constants based on the experience gathered in previous experimental investigations on similar soils. Although such a choice necessarily introduces a certain degree of subjectivity in the comparative evaluation of the model responses, it can still be considered acceptable for our purposes, considering that the typical range of variation of such parameters for different soils is relatively limited, and the model response is not very sensitive to their variation, see *e.g.*, Niemunis and Herle (1997); Stallebrass (1990); Ingram (2000); Clayton and Heymann (2001); Mašín (2004).

It is important to note that, although the initial conditions of all the specimen belonging to a single stress probing "rosette" were nominally identical, some small differences in their

initial effective stress and void ratio have been observed for both initial states A and B. In all the simulations discussed in this and in the next section, the average values reported in Tab. II have been assumed.

	p_0 (kPa)	q_0 (kPa)	e_0 (–)
State A	147.3	0.0	0.746
State B	148.4	60.0	0.752

Table II. Initial conditions assumed for the two sets of stress–probing tests

4.1. Modified Cam–Clay model

In the Modified Cam–Clay model, the parameters N, and λ provide the position and the slope of the isotropic virgin compression line in the $(1+e)$:$\ln p$ plane, while the constant κ represents the slope of isotropic unloading/reloading lines in the same plane. Those constants have been determined using the results of the isotropic compression and extension probes, Tx128 and Tx127, as shown in Fig. 4a.

The value of the friction angle at critical state, φ_c, has been determined from the results of all the stress probes leading the material to failure (Tx121–Tx126). In Fig. 4b, these results are plotted in terms of mobilized friction angle

$$\varphi_{\mathrm{mob}} := \sin^{-1}\left\{\frac{\sigma_1 - \sigma_3}{\sigma_1 + \sigma_3}\right\}$$

as a function of the deviatoric strain norm $|\epsilon_s|$. From the figure it is apparent that critical state conditions are attained at approximately the same friction angle in all the probes considered. From the results shown in the figure, a value of $\varphi_c = 33°$ has been selected. The critical state

stress ratio in triaxial compression, M, can be easily determined from φ_c by considering that

$$M = \frac{6 \sin \varphi_c}{3 - \sin \varphi_c}$$

The elastic shear modulus G was evaluated by trial and error, starting from the results of the p = const. compression probe (Tx126), as shown in Fig. 4c. From the results shown in the figure, a value of $G = 5$ MPa was adopted. The complete set of parameters for the Modified Cam–Clay model is summarized in Tab. III.

N (–)	λ (–)	κ (–)	M (–)	G (MPa)
2.245	0.097	0.017	1.33	5.0

Table III. Parameters of the Modified Cam–Clay model.

As for the initial conditions, it is worth noting that, due to the creep strains accumulated before the stress probing, the average e_0 value assumed for the specimens (reported in Tab. II) is slightly lower than the void ratio on the virgin compression line calculated for $p = p_0$ with the N and λ values given in Tab. III. Therefore, the initial value of the preconsolidation pressure p_{c0} (*i.e.*, the size of the elliptical yield locus along the isotropic axis) is slightly larger than p_0 and the soil appears as slightly overconsolidated ("quasi–preconsolidation" effect). The value of p_{c0} consistent with the assumed position of the virgin compression line and initial void ratio can be computed by the following equation:

$$1 + e_0 = N - \lambda \ln p_{c0} + \kappa \ln \frac{p_{c0}}{p_0} \tag{4.1}$$

with p_0 and e_0 provided by Tab. II and N, λ and κ as in Tab. III.

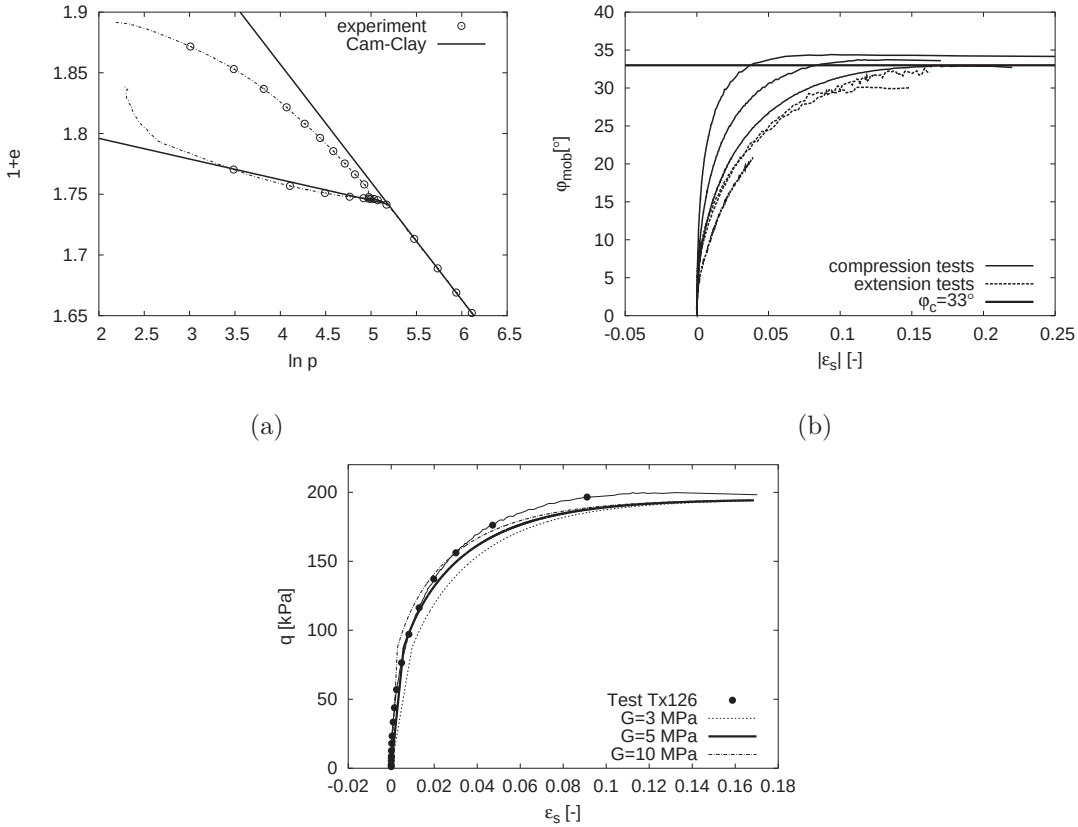

Figure 4. Calibration of the Modified Cam-Clay model: a) determination of parameters N, λ and κ from isotropic compression and extension probes; b) determination of critical state friction angle φ_c, from probes leading to failure; c) determination of elastic shear modulus, G, from the p = const. compression probe.

4.2. 3–SKH model

In the 3–SKH model, the material constants λ^* and N^* define the slope and position of the virgin compression line in the $\ln(1+e)$:$\ln p$ plane. Their numerical values have been determined by interpolating the experimental data from the isotropic compression probe, Tx128, shown in Fig. 4a.

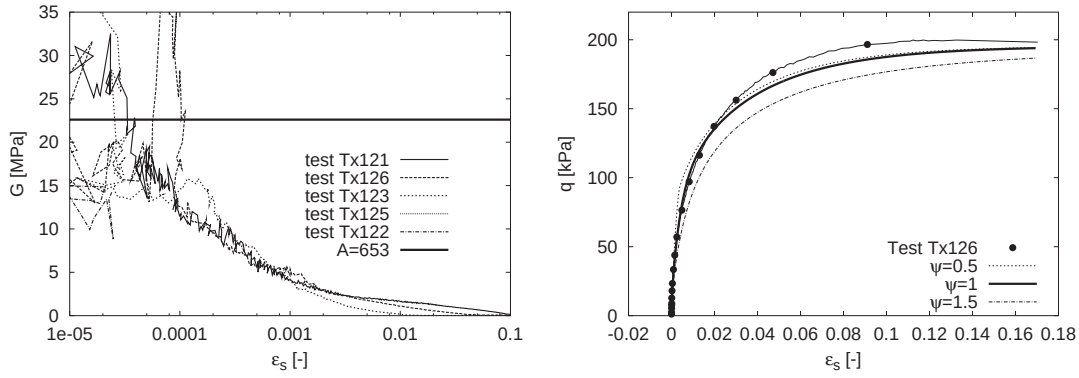

(a) (b)

Figure 5. Calibration of the 3–SKH model: a) determination of parameter A from deviatoric probes; b) determination of parameter ψ from the p = const. compression probe.

According to eq. $(6.17)_2$ of Appendix B, the constants A, m and n quantify the dependence of the elastic shear modulus G on mean effective stress p and preconsolidation pressure $2a$ (size of the Bounding Surface along the isotropic axis). Due to the lack of reliable information on the influence of such state variables on G, the values for the constants m and n have been set equal to those provided by Mašín (2004) for London Clay. The constant A was determined by comparing the shear stiffness value predicted by eq. $(6.17)_2$ with the tangent shear moduli measured in a number of deviatoric probes (Tx121–Tx123, Tx125 and Tx126) at very small strain levels. These tangent shear moduli are plotted in Fig. 5a as a function of the deviatoric strain. From the figure, it is apparent how the experimental data in the very small strain range ($\epsilon_s < 1.0 \cdot 10^{-4}$) are quite scattered, due to the lack of accurate strain measurements. For the purpose of model calibration, the average value $A = 653$ was selected, which is well inside the range of values reported for similar soils.

The constant κ^* controls the value of the bulk modulus of the material in the elastic range, see eq. $(6.17)_3$. In principle, it could be determined from the isotropic extension probe, Tx127,

as the slope of the tangent to the unloading curve in the $\ln(1+e)$:$\ln p$ plane at very small volumetric strains. However, due to the lack of accurate volume change measurements in the very small strain range, κ^* was determined from the elastic shear stiffness, as:

$$\kappa^* = \frac{p}{K} = \frac{3(1-2\nu)}{2(1+\nu)}\,\frac{p}{G}$$

by assuming a value of the Poissons ratio $\nu = 0.25$, at $p = 150$ kPa.

The parameter M, controlling the slope of the Critical State Line for axisymmetric compression in the q:p plane can be assumed equal to 1.33, as for the Modified Cam–Clay model. No ad–hoc experimental tests were performed to calibrate the parameters T and S. Therefore, in lack of sufficient information and since the values reported in the literature for these two constants lie in a very narrow range – see Stallebrass (1990); Baudet (2001); Ingram (2000); Mašín (2004) – the values determined by Mašín (2004) for London Clay were adopted.

The last material constant of the model – namely the exponent ψ appearing in the expression of the hardening moduli H_1 and H_2, eq. (6.34) – was determined by trial and error, by comparing the model response with the experimental results obtained in the p = const. compression probe Tx126. From the results shown in Fig. 5b, a value of $\psi = 1.0$ has been considered appropriate.

The complete set of parameters for the 3–SKH model is summarized in Tab. IV.

N^*	λ^*	A	n	m	κ^*	M	T	S	ψ
0.85	0.057	653	0.71 †	0.27 †	0.004	1.33	0.24 †	0.16 †	1.0

Table IV. Parameters of the 3–SKH model. Quantities indicated with the symbol † have been assumed from data reported by Mašín (2004) for London Clay.

The definition of the initial conditions requires the determination of the initial values of the

internal variable a – controlling the size of the elliptic Bounding Surface, see eq. (6.21) – and of the two back–stresses, $\boldsymbol{\sigma}_a$ and $\boldsymbol{\sigma}_b$, defining the centers of the yield surface and history surface, respectively (see Fig. 3).

As previously discussed in sect. 4.1, the initial state of the material appears to be slightly overconsolidated due to the quasi–preconsolidation effect induced by creep strains. In defining the initial value of the parameter a, this effect can be easily taken into account by fixing the position of the virgin compression line of the material. From the expressions of the virgin compression and unloading/reloading curves in the $\ln(1+e)$:$\ln p$ plane, the following relation between a and the initial void ratio e_0 and mean stress p_0 can be derived:

$$\ln(1+e_0) = N - \lambda^* \ln 2a + \kappa^* \ln \frac{2a}{p_0} \tag{4.2}$$

Eq. (4.2) can be solved for a, with p_0 and e_0 provided by Tab. II and N^*, λ^* and κ^* as in Tab. IV.

On the contrary, it is not clear how the back stresses $\boldsymbol{\sigma}_a$ and $\boldsymbol{\sigma}_b$ should evolve with creep strain. This introduces some uncertainty in the definition of the initial conditions, which must be considered in the evaluation of the model predictions. In order to assess the potential effect of the assumed initial conditions on the predicted directional behavior of the model, three possible scenarios were considered:

- Case 1: History surface and yield surface touch each other at the current stress state, and are both located at its left, as shown in Fig. 6a;
- Case 2: History surface and yield surface both centered about the current stress state: $\boldsymbol{\sigma} = \boldsymbol{\sigma}_a = \boldsymbol{\sigma}_b$;
- Case 3: History surface is in contact with the Bounding Surface at the isotropic stress state $p = 2a$; yield surface touches the current stress state and is located at its right, as

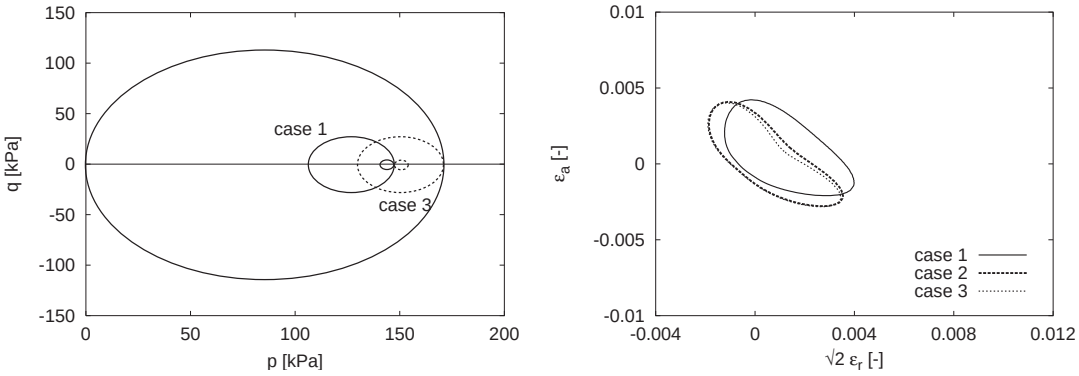

(a) (b)

Figure 6. Effect of initial position of kinematic hardening surfaces on the directional response of 3–SKH model. a) Initial positions of kinematic surfaces assumed for Cases (1) and (3); Strain response envelopes for axisymmetric probes from initial state A, and $R_\sigma = 50$ kPa.

shown in Fig. 6a;

The strain response envelopes obtained for Cases 1–3 under axisymmetric probes with $R_\sigma = 50$ kPa, starting from initial state A, are shown in Fig. 6b. While the results obtained for Cases (2) and (3) are almost coincident, some quantitative differences are apparent between the response envelopes for Cases (1) and (2). This is due to the fact that, in Case (1), plastic loading conditions with relatively low values of the plastic modulus occur even at very small strain levels in all the probes characterized by a net increase in mean stress p, whereas in the other two cases the response of the material in the very small strain range is always elastic or almost elastic.

In the following, the assumption made in Case (1) – i.e., that the quasi–preconsolidation due to creep affects only the sizes of the three surfaces, but not the position of history and yield surfaces with respect to the current stress state – has been assumed both for the calibration of the 3–SKH model and for the simulation of the stress probing experiments from state B,

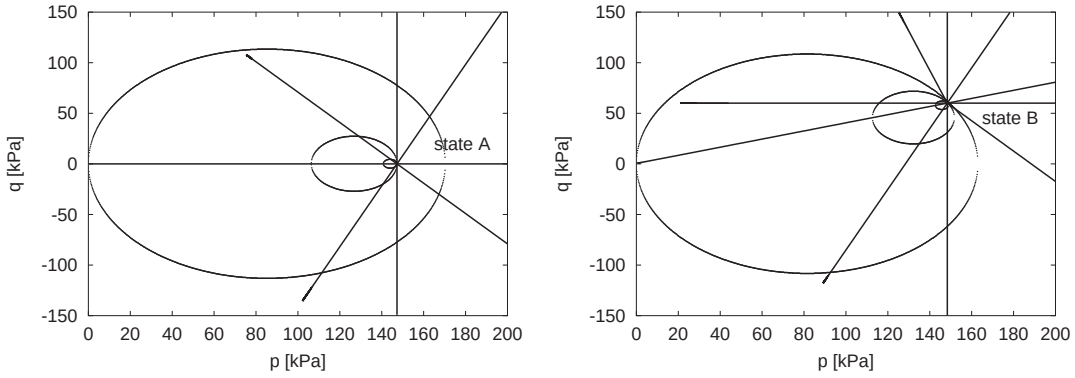

(a) (b)

Figure 7. Initial configuration assumed for the kinematic surfaces of 3–SKH model: a) initial state A; b) initial state B. Stress probe directions are also shown in the figures.

discussed in Sect. 5. The initial configuration assumed for the kinematic surfaces for states A ad B is shown in Fig. 7. Note that, while the state A appears as slightly overconsolidated, according to the value of the average initial void ratio reported in Tab. II, the state B lies on the Bounding Surface. The initial configuration of the kinematic hardening surfaces at state B, shown in Fig. 7b, is the only possible under the assumption of Case (1), due to the non–intersection condition. However, it is worth recalling that Clayton and Heymann (2001) report experimental evidence showing an initially stiff, "elastic" behavior after some period of rest.

4.3. CLoE hypoplastic model

As discussed by Chambon et al. (1994), the calibration of the CLoE model requires experimental data from some prescribed "basic paths", including:

i) conventional drained triaxial compression and extension;

ii) isotropic compression or extension;

iii) "pseudo–isotropic" (*i.e.*, isotropic loading from an anisotropic stress state) compression

and extension.

Four of these basic paths are included among the stress probes originating from the isotropic initial state A (Tx121, Tx122 and Tx127 or Tx128). As for the pseudo–isotropic tests, use was made of the results of the stress probe Tx115, originating from the initial state B. This is the only case in which some information from the stress–probing experiments conducted from the anisotropic state B was used in the calibration process.

The various constants of the CLoE model cannot be evaluated directly from the experimental results, since care must be taken in preserving the consistency of the constitutive tensors at isotropic states and on the limit surface, which bounds the region of admissible stress states in stress space. Rather, a complex calibration procedure must be followed in order to obtain a consistent set of parameters, see Chambon et al. (1994) for details. In this case, the calibration procedure was carried out using a specifically designed software tool, kindly provided by J. Desrues (2004). The results of the calibration process are summarized in Tab. V, providing the complete set of parameters adopted in the simulations with the CLoE model.

φ_c (deg)	c (kPa)	χ_{ca} (–)	y_{ca} (–)	y_{rc} (–)	p_{fc} (–)	p_{ref} (kPa)	$\epsilon_{v,\mathrm{ref}}$ (–)	λ_c (–)	φ_e (deg)
34.0	0	0.17	0.055	3.1	0	147.26	0.0	183.34	33

χ_d (–)	χ_c (–)	χ_{m2} (–)	y_e (–)	p_{fe} (–)	m_c (–)	m_e † (–)	n † (–)	ω † (–)	
-1.0	-0.1	-0.05	0.011	0.02	-0.2	0.0	-0.2	0.36	

Table V. Parameters of the CLoE model. Quantities indicated with the symbol † have been estimated according to Desrues (2004).

The comparison between model predictions and material response observed on the calibration paths is shown in Fig. 8. The model provides a fairly good match with experimental results for all calibration paths, with the only exception of the isotropic compression path (Fig. 8c), for which the model significantly underestimates the compressibility of the soil. This clear limitation is due to the fact that, in its current version, the model does not allow to prescribe independently the bulk and shear tangent moduli (in both compression and extension) at isotropic states, see Mašín et al. (2005). A change in the bulk stiffness in isotropic compression is reflected in the deviatoric response, so that any attempt to improve the model response in isotropic compression would unavoidably deteriorate the performance of the model along the other paths. The set of parameters shown in Tab. V was taken as the best possible compromise in terms of predictive capability of the model along the entire set of basic paths.

4.4. K–hypoplastic models for clays

A detailed discussion of the procedures required for the calibration of the K–hypoplastic model for clays can be found in Mašín (2005). The standard version of the model is fully characterized by five constitutive constants, namely N^*, λ^*, κ^*, φ_c and r.

The constants N^* and λ^* control the position and slope of the isotropic normal compression line in the $\ln(1+e)$:$\ln p$ plane. As such, they have the same physical meaning as the corresponding constants of the 3–SKH model (Sect. 3.1), and can be determined as discussed in Sect. 4.2. For the determination of the constant κ^* – which controls the compressibility of the soil in isotropic unloading – the choice has been made to use the results of the stress probe Tx127 in the medium strain range. A reasonably good fit to the available experimental data

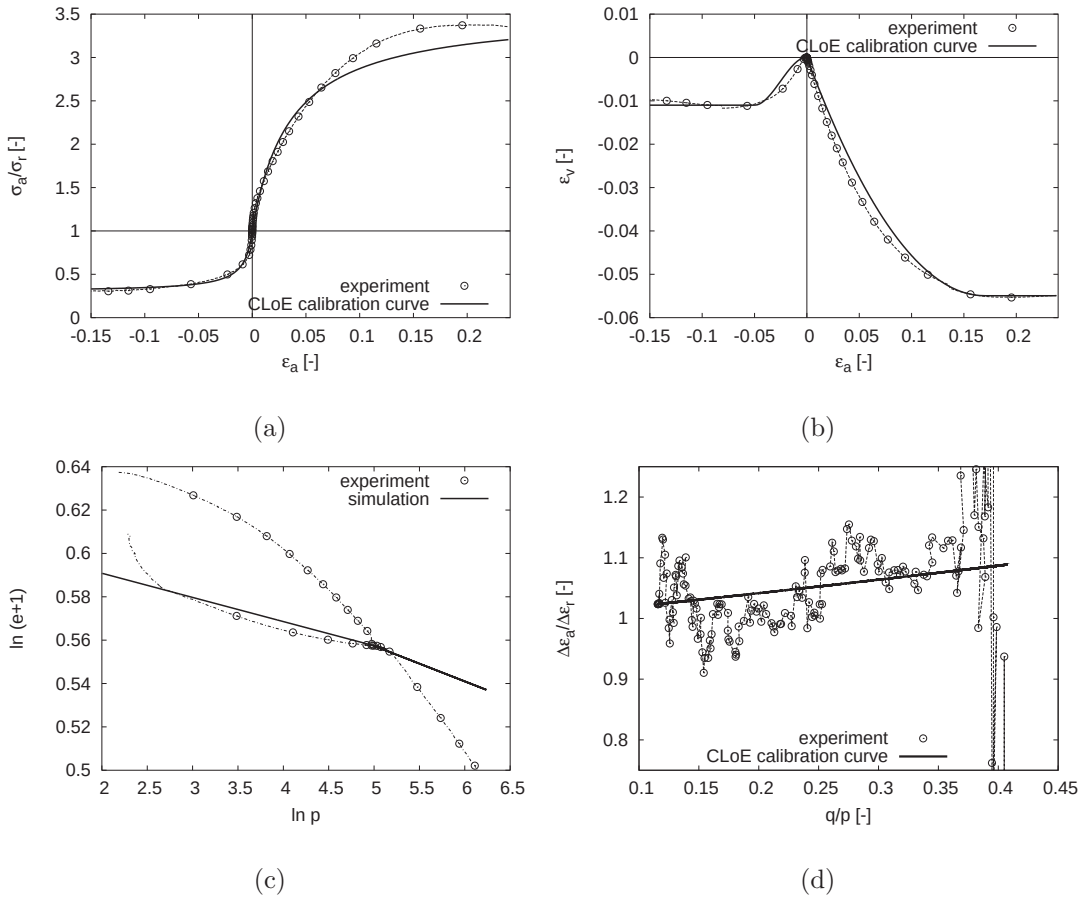

Figure 8. Calibration of the CLoE model: comparison of predicted and observed response for: a) conventional triaxial compression and extension tests, in the σ_a/σ_r:ϵ_a plane; b) conventional triaxial compression and extension tests, in the ϵ_v:ϵ_a plane; c) isotropic compression and extension probes, in the $\ln(1+e)$:$\ln p$ plane; d) pseudo–isotropic compression test, in the $\Delta\epsilon_a/\Delta\epsilon_r : q/p$ plane.

was obtained with $\kappa^* = 0.007$, as shown in Fig. 9a.

The constant φ_c defines the friction angle of the material in critical state conditions. Its determination has been already discussed in Sect. 4.1. The last constant, r, controls the ratio between shear and bulk stiffness in isotropic virgin states. It was calibrated by trial and error, by comparing the model response with the experimental data from the stress probe Tx126,

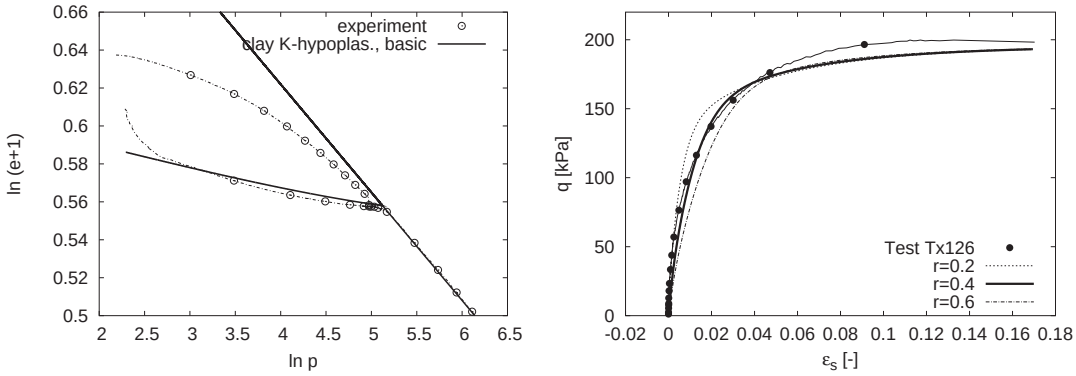

(a) (b)

Figure 9. Calibration of the K–hypoplastic model for clays: comparison of predicted and observed response for: a) isotropic compression and extension tests, in the $\ln(1+e)$:$\ln p$ plane; b) constant p triaxial compression, in the q:ϵ_s plane.

i.e., a constant p compression test from the isotropic virgin state A. The best fit between predictions and measurements was obtained with $r = 0.4$, see Fig. 9b.

The extension of the K–hypoplastic model to include the effects of previous loading history by means of the intergranular strain concept requires five additional constants to be identified, namely m_R, m_T, R, β_r and χ (see Niemunis and Herle, 1997). In principle, their calibration requires experimental data from non–conventional laboratory experiments involving complex loading paths – such as those considered by Atkinson et al. (1990) in the experimental evaluation of the effects of recent stress history – and small–strain stiffness measurements using dynamic testing techniques. Such experiments are not included in the experimental program considered in this study. However, as suggested by Mašín (2005), the constants R, β_r and χ, which provide the extent of the quasi–elastic range for the material and the stiffness degradation rate with increasing strain, typically show a relatively limited range of variation for different soils, and therefore have been estimated with reference to the experimental data

available for London Clay (Mašín, 2004).

The constant m_R, which controls the hypo–elastic stiffness upon stress path reversal in the very small strain range, was estimated by means of the following relation between m_R and the small–strain shear modulus G_0 in isotropic conditions (Mašín, 2005):

$$G_0 \simeq \frac{m_R p}{r\lambda^*} \qquad \Leftrightarrow \qquad m_R \simeq \frac{G_0 r\lambda^*}{p} \tag{4.3}$$

with $G_0 = 23.0$ MPa at $p = 150$ kPa, see Fig. 5a. This guarantees that the enhanced K–hypoplastic model and the 3–SKH model are characterized by identical shear stiffnesses in the very small strain range. Finally, in the absence of any other experimental indication, m_T was assumed equal to m_R. The results of the calibration process are summarized in Tab. VI.

N^* (–)	λ^* (–)	κ^* (–)	φ_c (deg)	r (–)	m_R (–)	m_T (–)	R (–)	β_r (–)	χ (–)
0.85	0.057	0.007	33.0	0.4	3.5	3.5	10^{-4} †	0.2 †	6.0 †

Table VI. Parameters of the K–hypoplastic models for clays. Quantities indicated with the symbol † were assumed from data reported by Mašín (2004) for London Clay.

The definition of the initial conditions requires the determination of the initial values of the void ratio and of the intergranular strain tensor $\boldsymbol{\delta}$. As for the void ratio, the values provided in Tab. II were adopted. Note that, with the values of N^* and λ^* given in Tab. VI, the void ratio assumed for the isotropic state A is slightly lower than the void ratio on the virgin compression line at the same mean stress. This implies that the material appears slightly overconsolidated, as already noted in Sect. 4.2. The initial values of the intergranular strain for the two states A and B were determined by numerically simulating the two constant q/p compression paths imposed to the material before the start of the stress–probing. This guarantees that the initial

values of $\boldsymbol{\delta}$ are consistent with the initial configuration of the kinematic surfaces in the 3–SKH model.

5. COMPARISON OF OBSERVED AND PREDICTED RESPONSE

5.1. Strain response envelopes

In the following, the response of reconstituted Beaucaire Marl to the stress probing program detailed in Tab. I, as well as the predictions of the different models described above, is depicted by using the so–called *incremental strain response envelope*, as defined in Tamagnini et al. (2002). Such a representation directly follows from the concept of stress response envelope, first proposed by Gudehus (1979) as a convenient tool for visualizing the properties of rate-type constitutive equations. According to Gudehus, a stress (strain) response envelope is defined as the image in the stress (strain) rate space of the unit sphere in the strain (stress) rate space, under the map defined by the constitutive equation. By simply replacing rates with finite-size increments, the same definitions apply to the incremental response envelopes. In the general case, an incremental strain response envelope (RE, hereafter) is a surface in a six-dimensional space. However, for the particular loading conditions considered, the most natural choice is to represent the section of the REs in the plane of work-conjugated strain increment quantities, $(\Delta\epsilon_a, \sqrt{2}\,\Delta\epsilon_r)$, see Fig. 1b. The size of each strain increment vector defining the RE can be directly interpreted as a directional secant compliance of the material, for the associated loading direction and stress increment magnitude.

Figures 10 and 11 show the computed REs for all the models considered at small to medium stress increment levels (R_σ = 20, 30, 40 and 50 kPa), and at medium to large stress increment

levels (R_σ = 50 and 90 kPa), respectively. The corresponding experimentally obtained REs are also shown in both figures on the top left corner.

For small to medium stress increment levels, the experimental REs indicate that the softest response is associated with those paths which are characterized by a large deviatoric component (*e.g.*, tests Tx119 and Tx113). As R_σ increases, the envelopes progressively shift upward to the left, due to the fact that the initial state is closer to the critical state line for axisymmetric compression than to the corresponding line for axisymmetric extension. For $\eta = 0.4$ loading paths (Tx130 and Tx129), the material response is softer when the probe points in the direction of continued loading, and stiffer upon unloading (*i.e.*, upon full stress path reversal with respect to the consolidation history). In fact, this last path corresponds to the stiffest response of the material. A direct consequence of the above observations is that the experimental REs are markedly non–symmetric about the origin of the strain increment space.

The predictions of the different models considered appear, from a qualitative standpoint, all in fair agreement with the salient features of the experimental response discussed above. The only notable exception is represented by the predictions of CLoE model upon $\eta = 0.4$ loading paths, where – contrary to experimental evidence – no significant difference between secant stiffness in compression and extension is observed. From a quantitative standpoint, however, all models appear to significantly underpredict the secant stiffness of the material. The REs predicted with the two elastoplastic models show a convex shape, except for the expected, yet minor irregularity of the Modified Cam–Clay envelopes, close to neutral loading in extension. The REs of the two K–hypoplastic models, and (to a much lesser extent) those of CLoE show some degree of non–convexity in a region located around the $\eta = 0.4$ loading direction. This feature is also shown by the two largest experimental REs, although such an observation is

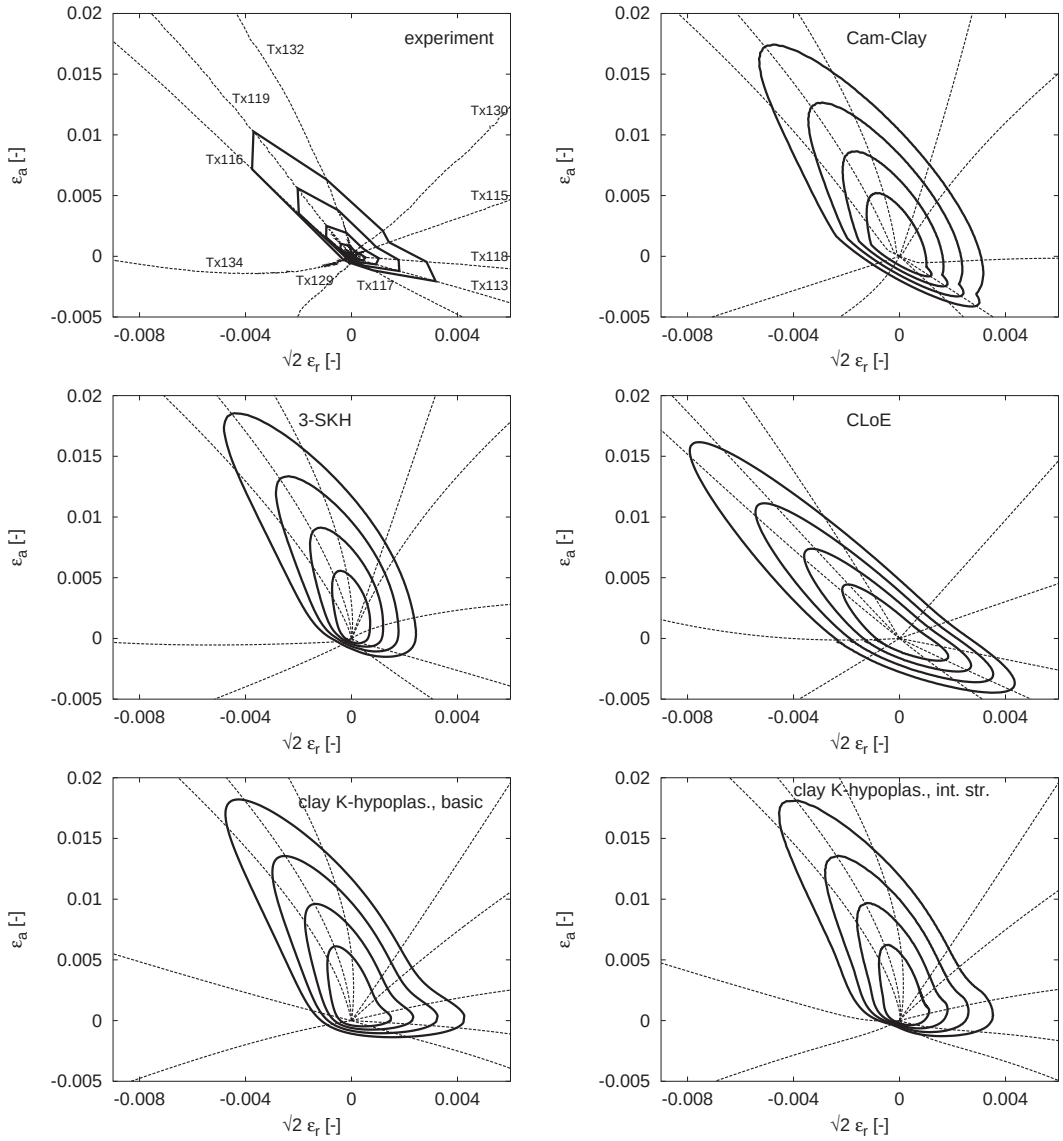

Figure 10. Experimental *vs.* simulated strain response envelopes for $R_\sigma = 20$, 30, 40 and 50 kPa

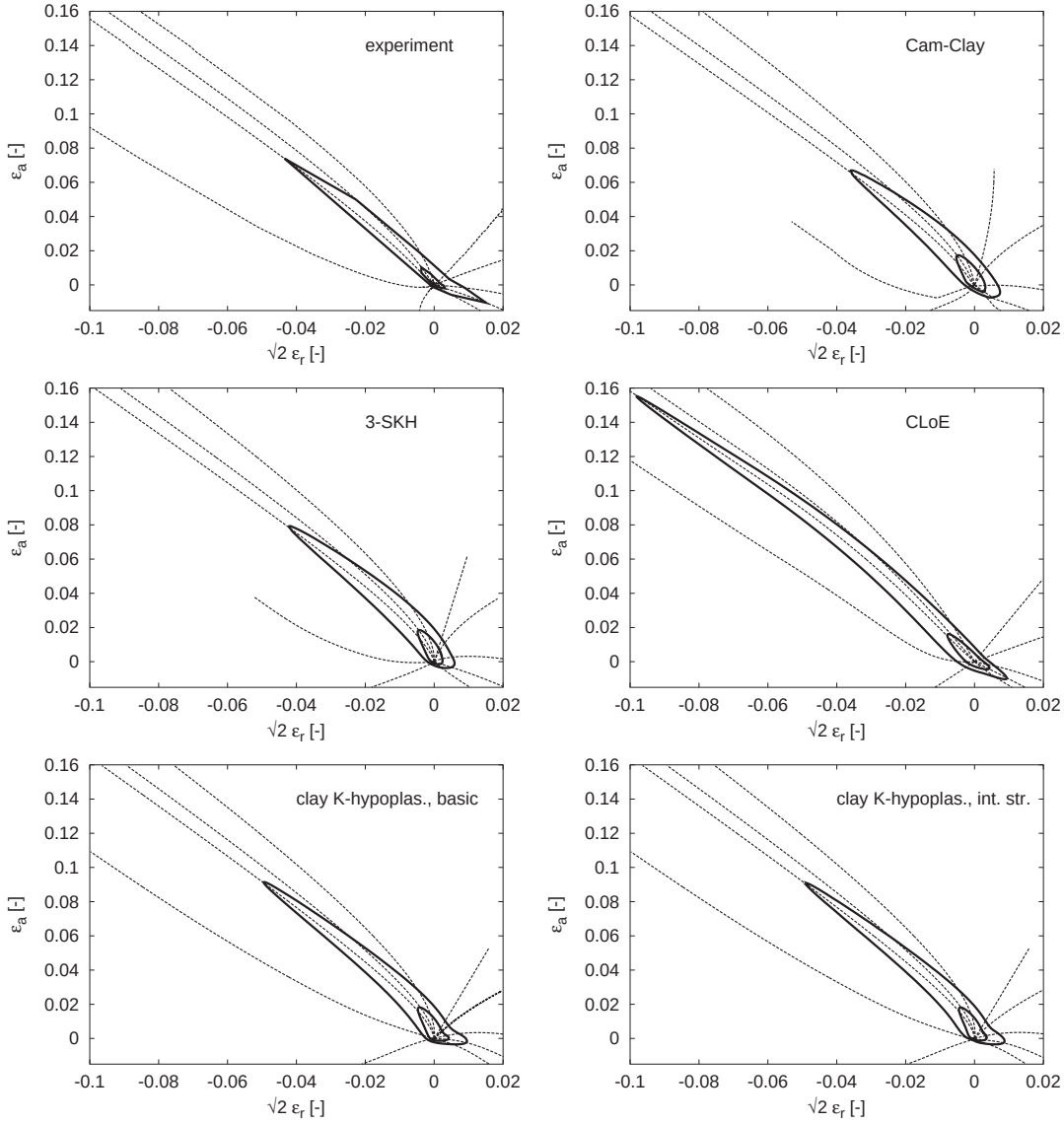

Figure 11. Experimental *vs.* simulated strain response envelopes for $R_\sigma = 50$, and 90 kPa

based on the results of one single stress–probe.

At large stress increment level (R_σ = 90 kPa, Fig. 11), both the elastoplastic and the K–hypoplastic models provide response envelopes which appear in fairly good agreement with the experimental results, from both a qualitative and a quantitative point of view. On the contrary, CLoE significantly overestimates soil stiffness for loading paths close to deviatoric compression (Tx116 and Tx119).

5.2. Normalized stress–paths

In addition to response envelopes, the performance of the five models can be also assessed by representing the prescribed stress paths in the normalized plane $q/p_e^* : p/p_e^*$, where p_e^* is the equivalent pressure, given by:

$$p_e^* := \exp\left\{\frac{N-1-e}{\lambda}\right\} \qquad \text{for Modified Cam–Clay;} \tag{5.1}$$

$$p_e^* := \exp\left\{\frac{N^*-\ln(1+e)}{\lambda^*}\right\} \qquad \text{otherwise.} \tag{5.2}$$

Figure 12 shows such normalized stress–paths for both the constitutive models and the actual experiments. For the latter, the equivalent pressure was evaluated using eq. (5.2).

For the two elastoplastic models, the normalized stress–paths clearly define a single limit surface – of nearly elliptic shape – in the normalized plane, due to the isotropic volumetric hardening law adopted to describe the evolution in size of the Bounding Surface of the material (coinciding with the yield surface for the Modified Cam–Clay model). It is worth noting that the initial portion of the experimental stress–paths Tx115, Tx130 and Tx132 show a sharp bend which can be attributed to a quasi–preconsolidation effect similar to the one observed for the initial state A. This effect is not captured by the two elastoplastic models, due to an inadequate characterization of the initial state.

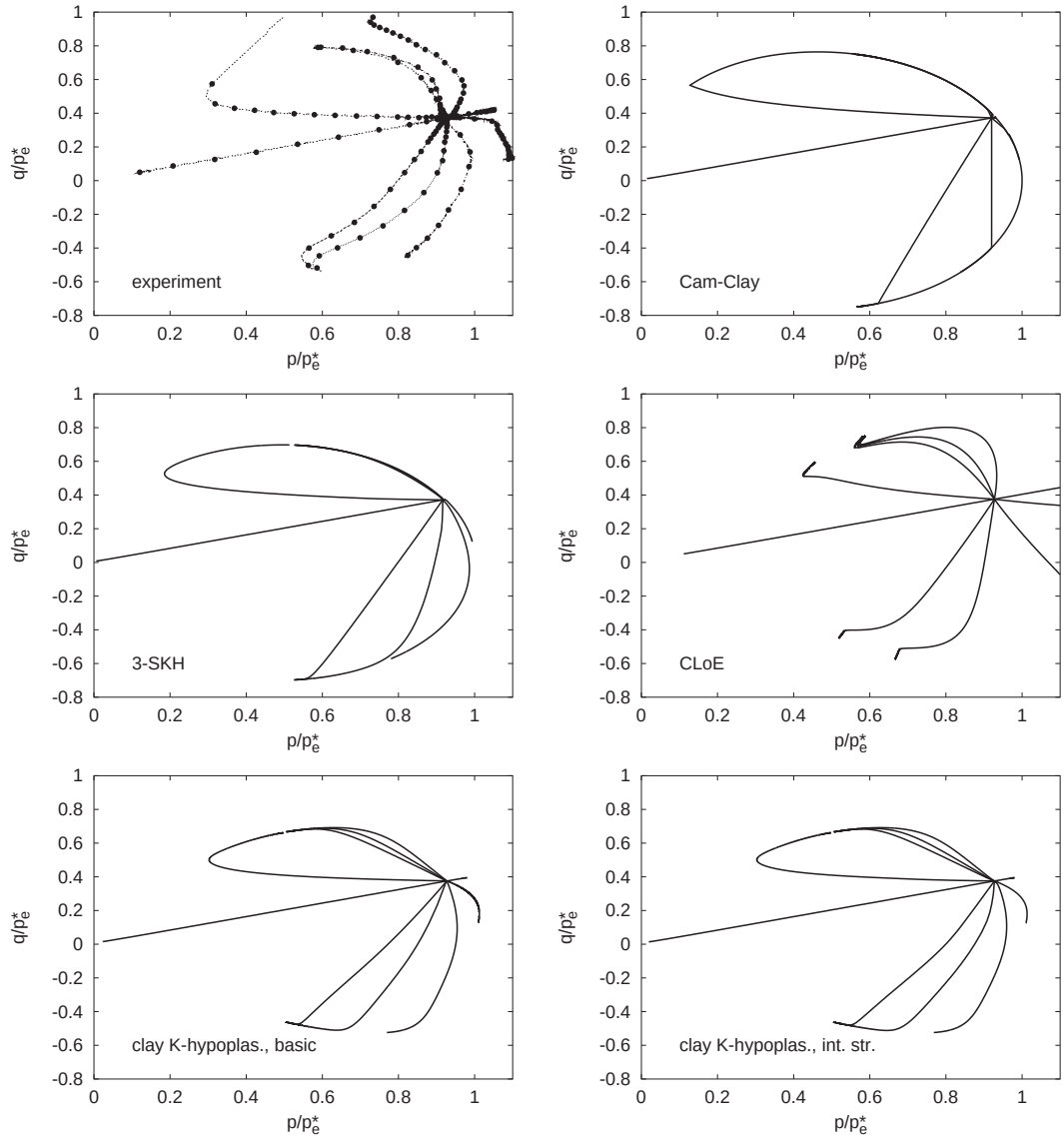

Figure 12. Experimental *vs.* simulated stress paths in the normalized plane q/p_e^*:p/p_e^*.

Interestingly, the response predicted by the two K–hypoplastic models is quite satisfactory when compared to the experimental data, although no such concept as a Bounding Surface is introduced in their formulation. The appearance of a state boundary surface in the model predictions is, in this case, a combined effect of the assumed barotropy and pyknotropy functions, which endow this particular version of K–hypoplasticity with a single critical state line and a unique virgin isotropic compression line (Mašín and Herle, 2005).

The response of CLoE model is somewhat different from that of all the other models considered in two respects. First, although the response along essentially deviatoric stress paths (probes Tx116, Tx119, Tx132, Tx117 and Tx113) is in reasonable agreement with the data, the normalized stress paths do not converge towards a unique point, which is consistent with the absence of the concept of a critical state line in the model formulation. Second, the performance of CLoE appears quite poor for stress–paths in the region bounded by probes Tx118 and Tx130. This is due to the same factors which originate the problems observed when calibrating the model response along a purely isotropic compression path.

5.3. Accuracy of directional predictions

While the strain response envelopes plotted in Figs.10 and 11 provide a clear qualitative picture of the performance of the five models considered, a more quantitative comparison of model predictions can be obtained by introducing a suitable scalar measure of the "distance" between model response and experimental results.

Herein, the following quantities have been adopted. Let the quantities α_σ^{pq} denote the orientation of the generic stress probe of size R_σ in the q:p plane, and let the stress probe be subdivided into N increments, of length $\Delta R_\sigma = R_\sigma/N$. Then, for each model, the simulation

error $\mathrm{err}(\alpha_\sigma^{pq}, R_\sigma)$ can be defined as:

$$\mathrm{err}(\alpha_\sigma^{pq}, R_\sigma) = \sum_{k=1}^{N} \left\| \Delta\boldsymbol{\epsilon}_{\mathrm{sim}}^{(k)} - \Delta\boldsymbol{\epsilon}_{\mathrm{exp}}^{(k)} \right\| \tag{5.3}$$

where $\Delta\boldsymbol{\epsilon}_{\mathrm{exp}}^{(k)}$ and $\Delta\boldsymbol{\epsilon}_{\mathrm{sim}}^{(k)}$ are the measured and predicted strain increment tensors, respectively, corresponding to the k–th stress increment of size ΔR_σ.

To assess the relative size of the prediction error, as compared to the strain–path length, a second, normalized error measure is introduced as follows:

$$\mathrm{err}_{\mathrm{norm}}(\alpha_\sigma^{pq}, R_\sigma) = \frac{\mathrm{err}(\alpha_\sigma^{pq}, R_\sigma)}{\sum_{k=1}^{N} \left\| \Delta\boldsymbol{\epsilon}_{\mathrm{exp}}^{(k)} \right\|} \tag{5.4}$$

Figures 13 and 14 show computed values of err and $\mathrm{err}_{\mathrm{norm}}$ as a function of the probe direction α_σ^{pq}. Two stress increment ranges have been considered, namely $R_\sigma = 30$ kPa (Fig. 13) and $R_\sigma = 90$ kPa (Fig. 14). In both cases, the evaluation of the two error measures has been carried out with $\Delta R_\sigma = 5$ kPa, which was considered to be the smallest stress increment for which experimental results are not significantly affected by scatter in the measurements.

For $R_\sigma = 30$ kPa, the performance of the two elastoplastic models is compared in Fig. 13a. The largest prediction error, err $\simeq 0.006$, corresponds to probe directions with α_σ^{pq} around 72° (conventional triaxial compression). This is a consequence of the fact that, while the initial state for the two models lies on the Bounding Surface, the experimental data clearly indicate that the soil possesses some degree of overconsolidation (see Fig. 12), probably induced by creep strains accumulated during the rest period before probing. The best predictions, in absolute terms, are obtained in the range $200° < \alpha_\sigma^{pq} < 300°$. This is not surprising, since in this region the response of the two models is quite stiff, hence the strain increment magnitudes are quite small. The effect of loading direction is less important when considering the relative error, $\mathrm{err}_{\mathrm{norm}}$, as this quantity accounts for the dependence of soil stiffness on loading direction. The two models

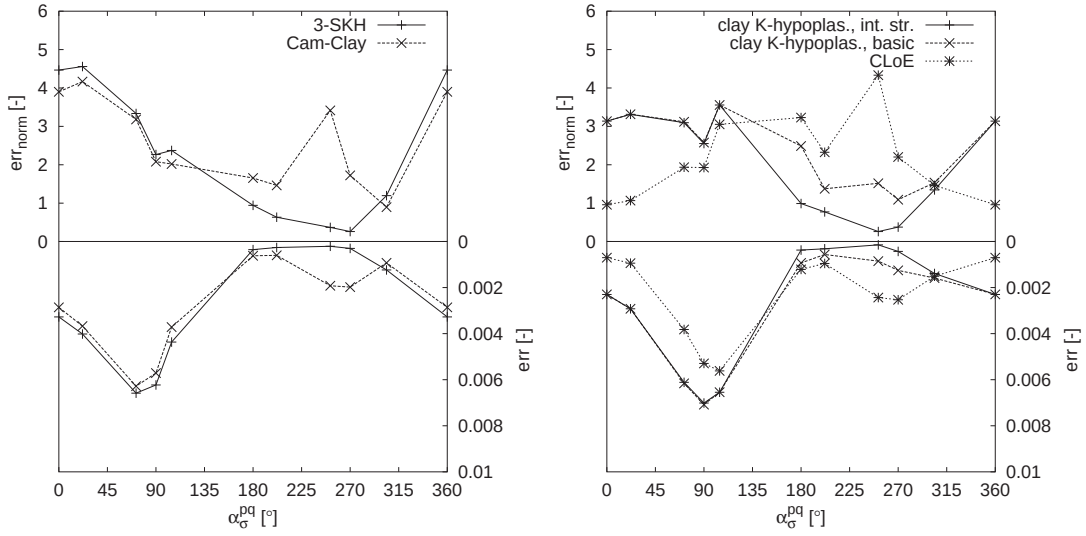

(a) (b)

Figure 13. Scalar error measures with respect to the stress–path direction α_σ^{pq} in the p:q plane at state B, $R_\sigma = 0 - 30$ kPa

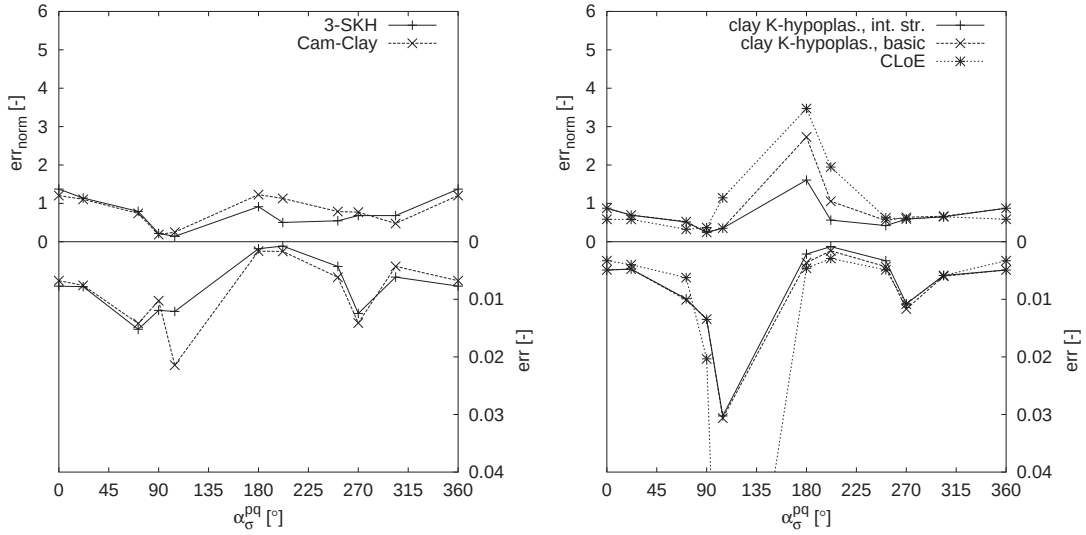

(a) (b)

Figure 14. Scalar error measures with respect to the stress–path direction α_σ^{pq} in the p:q plane at state B, $R_\sigma = 0 - 90$ kPa

provide almost identical predictions for the entire range of probing directions, except for the zone in which Modified Cam–Clay undergoes elastic unloading ($200° < \alpha_\sigma^{pq} < 300°$). Again, this is to be expected, since when the initial state is on the Bounding Surface, the 3–SKH model behaves as a standard Modified Cam–Clay for all probes which are directed outwards. On the contrary, when the stress–probes are directed inwards, then the more evoluted nested surface kinematic hardening structure of the 3–SKH model is capable of reproducing much better the experimental response, in both absolute and relative terms.

For the same stress increment range, the performance of the hypoplastic models is shown in Fig. 13b. The computed absolute error distributions with probe direction are quite similar, both in shape and magnitude, to those of the two elastoplastic models. The same is also true, to a certain extent, for the normalized error. The response of the two K–hypoplastic models is almost coincident for those probes corresponding to continued loading conditions, as in this case the material reaches quite rapidly the swept–out–memory conditions. Under reverse loading conditions, the two responses diverge and, as expected, the K–hypoplastic model with intergranular strains performs significantly better. This is even more apparent when considering the normalized error plots. For the same range of probe directions, CLoE performance appears to be substantially poorer, both in absolute and relative terms. On the contrary, for continued loading conditions ($340° < \alpha_\sigma^{pq} < 90°$) CLoE provides the best results among all the models considered. In fact, this is a consequence of a fortuitous combination of two different factors. On the one hand, CLoE calibration has clearly shown that the model is not capable of correctly reproducing the large decrease in stiffness associated with virgin loading upon isotropic or $\eta =$ const. loading conditions. On the other hand, the actual response of the material for the same range of probing directions appears to be much stiffer than expected for a material in a

virgin state, due to the quasi–preconsolidation effect already mentioned.

Overall, data reported in Fig. 13 indicate that the best performance is provided by the 3–SKH model and the K–hypoplastic model with intergranular strains, which appear to yield quite similar results in terms of prediction error measures. A somehow different picture emerges by looking at the results for the larger stress increment range (Fig. 14). In this case, not only the relative error levels are generally lower, but also the differences between the models are less important. In fact, Modified Cam–Clay performs almost as well as the more refined 3–SKH model, and the same applies to all the hypoplastic models, except for loading directions close to $\alpha_\sigma^{pq} = 180°$. In this case, roughly corresponding to a reduction of mean stress at $q = \text{const.}$, CLoE performance is quite poor, while K–hypoplasticity with intergranular strain provides the best prediction among the models of this class, although not as good as those of the two elastoplastic models.

6. CONCLUDING REMARKS

The comparative evaluation of the performance of different constitutive models in their application to the quantitative solution of practical engineering problems is a very complex task, which – in general – requires a careful consideration of several key factors, among which we recall:

1. Qualitative and quantitative agreement between experimentally observed response and model predictions at the element level (*i.e.*, in the simulation of laboratory tests), in view of the main objectives of the analysis and the type of problem to be solved;
2. Relative complexity of the procedures required to determine the material constants

appearing in the model formulation;

3. Type and nature of the internal state variables entering the model to describe the effects of previous loading history, and the relative complexity in the characterization of their initial values;
4. Availability of robust and accurate algorithms for the numerical implementation in FE codes, in view of the solution of the engineering problems at hand.

The comparison between model predictions and experimental results is typically done, in practice, with reference to a limited number of more or less conventional stress paths, whereas the response of the material for different loading conditions is extrapolated in a more or less reasonable way. This can be quite sufficient to assess the model performance in those problems where most of the soil affected by the imposed loading conditions undergoes very similar stress paths, and one of such paths is included in the laboratory testing program. Unfortunately, this is only seldom the case in many important applications where an accurate prediction of soil–structure interaction processes and of the displacement field around the structure is required. Notable examples in this respect are provided by deep excavations and shallow tunnels to be realized in urban environments, as in such cases, different zones of soil experience widely different stress–paths, both in size and direction, and the quality of numerical predictions crucially relies on the ability of the constitutive model adopted for the soil to accurately reproduce the material response along *all* such loading paths.

In this paper, an attempt has been made to evaluate the response of different advanced constitutive models for fine–grained soils in more general terms, considering their predictive capabilities over a quite wide range of loading conditions. In trying to compare the performances of the different models, the experimental data of Costanzo et al. (2006) have

been considered as portraying the actual mechanical response of the soil. However, two main points should be stressed in this respect. First, due to the time required to perform each test, only a few probes were duplicated, and thus most of the data on which the experimental REs are constructed refer to a single specimen only. Therefore, the observed shape of the experimental REs might be affected to some extent by the unavoidable scatter always present in experimental measurements. Second, the occurrence of small amounts of viscous strains may affect both size and shape of the measured response envelopes, even if to a limited extent, see Costanzo et al. (2006). Interpreting the observed response in light of rate–independent constitutive theories might therefore lead to an underestimation of soil stiffness for some probe directions and to an overestimation of soil stiffness for other probe directions, as thoroughly discussed in the companion paper (Costanzo et al., 2006).

Based on the normalized stress paths reported in Sect. 5.2 and the scalar error measures introduced in Sect. 5.3, the best performance overall appears to be provided by the intergranular strain–enhanced K–hypoplastic model for clays and the 3–SKH model, at both small and large strain levels.

It is interesting to note that, since the soil considered in this study was in a (almost) normally consolidated state, the predictions of the classical Cam–Clay model for continued loading conditions (*i.e.*, those paths pointing outside the yield surface) are equivalent to those obtained with the much more sophisticated 3–SKH model. In unloading, however, the data clearly show the substantial improvement of predictions which can be achieved with the kinematic hardening approach.

As compared to its enhanced version, the performance of the standard K–hypoplastic model is still reasonably good, mainly because the loading programmes considered involve only a

very limited number of stress reversals. For the application to monotonic (or quasi–monotonic) loading conditions, the standard K–hypoplastic model may represents a valid alternative to more complex formulations.

On the contrary, the performance of the CLoE model is definitely poor, when compared with the other elastoplastic or hypoplastic models, particularly for those loading paths involving a significant increase in mean stress. This is not surprising, considering that CLoE is a first–generation hypoplastic model, in which the stress tensor is assumed as the only state variable for the material. For this reason, the mathematical structure of CLoE model does not allow to properly distinguish normally consolidated and overconsolidated states, and to correctly describe critical state failure conditions. While CLoE has demonstrated its capability of accurately modelling the response of coarse–grained soils along mainly deviatoric loading paths (see, *e.g.*, Chambon et al., 1994), these limitations obviously make it unfit to model the behavior of natural clay deposits. An attempt to modify the current version of CLoE in order to improve its performance for normally consolidated clays has been recently presented by Mašín et al. (2005).

Although the enhanced K–hypoplastic model and the 3–SKH model provide a great flexibility in describing the effects of recent stress history on the mechanical response of the soil, they are both characterized by a relatively limited number of constants, most of which are linked to standard features of clay behavior. All the constants appearing in these two models can be determined by means of standard laboratory tests, with the only exception of those controlling the stiffness of the material at very low strain levels. As discussed by Mašín (2005), these latter quantities can be easily determined from the results of dynamic tests, such as bender element or resonant column tests.

On the contrary, the CLoE model requires a much wider pool of experimental data to calibrate the large number of constants (19) appearing in the functions adopted to describe the material response along the selected basic paths. Moreover, as those parameters typically control more than one specific feature of the material response, they cannot be determined independently. Rather, they have to be found by means of a complex calibration procedure which has to be implemented numerically in a suitable calibration code. This represents a second, major drawback of the CLoE model as compared to the more recent K–hypoplastic models for clays.

The characterization of the initial state of the material is relatively easy for Modified Cam–Clay, CLoE and standard K–hypoplastic models, for which only the initial values of the stress tensor and (possibly) one additional scalar state variable (preconsolidation pressure or void ratio) are required. Defining the initial state is more complex for the enhanced K–hypoplastic model and the 3–SKH model, since it requires the determination of one or two tensorial internal variables (the back–stresses or the intergranular strain). Even in the simple case considered in this study, this has not been a trivial task. The difficulties experienced in the definition of the initial state have had an impact both on the results of the calibration procedures and on the prediction of the material response. It is reasonable to expect that such difficulties would increase in the application of those models to natural clay deposits, with a more complicated – and possibly unknown – previous loading history. In such a case – based on some experimental observations of Jardine et al. (1984) and Clayton and Heymann (2001), who report an increase in soil stiffness for all loading directions after a relatively short resting period – Niemunis and Herle (1997) suggest to assume $\boldsymbol{\delta} = \mathbf{0}$. This is equivalent to setting $\boldsymbol{\sigma}_a = \boldsymbol{\sigma}_b = \boldsymbol{\sigma}$ for the 3–SKH model.

Finally, as far as computational issues are concerned, it can be noted that robust and accurate implicit or explicit integration algorithms are now available for both complex plasticity models (see, *e.g.*, Borja et al., 2001; Rouainia and Wood, 2001; Luccioni et al., 2001) and advanced hypoplastic models (see, *e.g.*, Fellin and Ostermann, 2002; de Borst and Heeres, 2002). However, as the mathematical structure of the K–hypoplastic models appears simpler than that of the 3–SKH model, or of any other kinematic hardening multisurface plasticity model, the former may have some advantage with respect to the latter as far as their numerical implementation into existing FE codes is concerned.

ACKNOWLEDGEMENT

The first author gratefully acknowledges the financial support by the research grants GAAV IAA200710605 and SSPI-CT-2003-501837-NOAH'S ARK under the EC 6$^{\text{th}}$ FP.

References

Al Tabbaa, A., Wood, D. M., 1989. An experimentally based "bubble" model for clay. In: Proc. 3^{th} Int. Conf. on Numerical Models in Geomechanics. Niagara Falls.

Atkinson, J. H., Richardson, D., Stallebrass, S. E., 1990. Effects of recent stress history on the stiffness of over–consolidated soil. Géotechnique 40 (4), 531–540.

Baudet, B. A., 2001. Modelling effects of structure in soft natural clays. Ph.D. thesis, City University, London.

Borja, R. I., Lin, C.-H., Montans, F. J., 2001. Cam–clay plasticity, Part IV: Implicit integration of anisotropic bounding surface model with nonlinear hyperelasticity and ellipsoidal loading function. Comp. Meth. Appl. Mech. Engng. 190, 3293–3323.

Callisto, L., Calabresi, G., 1998. Mechanical behaviour of a natural soft clay. Géotechnique 48 (4), 495–513.

Chambon, R., Desrues, J., 1985. Bifurcation par localisation et non linéarité incrémentale: un example heuristique d'analyse complete. In: Plastic Instability. Presses ENPC, Paris, France.

Chambon, R., Desrues, J., Hammad, W., Charlier, R., 1994. CLoE, a new rate–type constitutive model for geomaterials. theoretical basis and implementation. Int. J. Num. Anal. Meth. Geomech. 18, 253–278.

Clayton, C. R. I., Heymann, G., 2001. Stiffness of geomaterials at very small strains. Géotechnique 51 (3), 245–255.

Costanzo, D., Viggiani, G., Tamagnini, C., 2006. Directional response of a reconstituted fine–grained soil. part i: Experimental investigation. Int. J. Num. Anal. Meth. Geomech. (accepted for publication).

Darve, F., 1990. The expression of rheological laws in incremental form and the main classes of constitutive equations. In: Darve, F. (Ed.), Geomaterials: Constitutive Equations and Modelling. Elsevier.

de Borst, R., Heeres, O., 2002. A unified approach to the implicit integration of standard, non-standard and viscous plasticity models. Int. J. Num. Anal. Meth. Geomech. 26, 1059–1070.

Desrues, J., 2004. Private communication.

Desrues, J., Chambon, R., 1989. Shear band analysis for granular materials: the question of incremental non–linearity. Ingenieur–Archiv 59, 187–196.

Fellin, W., Ostermann, A., 2002. Consistent tangent operators for constitutive rate equations. Int. J. Num. Anal. Meth. Geomech. 26, 1213–1233.

Finno, R. J., Harahap, I. S., Sabatini, P. J., 1989. Analysis of braced excavations with coupled finite element formulations. Comp. & Geotechnics 12, 91–114.

Graham, J., Noonan, M., Lew, K. V., 1983. Yield states and stress-strain relationships in natural plastic clay. Can. Geotech. J. 20, 502–516.

Grant, R. J., Stallebrass, S. E., Taylor, R. N., 1996. Prediction of pre-failure ground movements: Physical and numerical techniques. In: Proc. 14^{th} Int. Conf. Soil Mechanics and Foundation Engineering. Balkema Rotterdam.

Gudehus, G., 1979. A comparison of some constitutive laws for soils under radially symmetric loading and unloading. In: Wittke (Ed.), 3rd Int. Conf. Num. Meth. Geomech., *Aachen*. Balkema, Rotterdam.

Gudehus, G., 1996. A comprehensive constitutive equation for granular materials. Soils and Foundations 36 (1), 1–12.

Gudehus, G., Goldscheider, M., winter, H., 1977. Mechanical properties of sand and clay. In: Gudehus, G. (Ed.), Finite Elements in Geomechanics. John Wiley & Sons.

Hashiguchi, K., 1985. Two– and three–surface models of plasticity. In: V Int. Conf. Num. Meth. in Geomechanics. Balkema, Rotterdam, Nagoya, Japan.

Herle, I., Kolymbas, D., 2004. Hypoplasticity for soils with low friction angles. Computers and Geotechnics 31 (5), 365–373.

Ingram, P. J., 2000. The applicaton of numerical models to natural stiff clays. Ph.D. thesis, City University, London.

Jardine, R. J., Symes, M. J., B., B. J., 1984. The measurement of soil stiffness in the triaxial apparatus. Géotechnique 34, 323–340.

Kolymbas, D., 1991. An outline of hypoplasticity. Archive of Applied Mechanics 61, 143–151.

Lanier, J., Caillerie, D., Chambon, R., Viggiani, G., Bésuelle, P., Desrues, J., 2004. A general formulation of hypoplasticity. Int. J. Num. Anal. Meth. Geomech. 28, 1461–1478.

Lewin, P. I., Burland, J. B., 1970. Stress-probe experiments on saturated normally consolidated clay. Géotechnique 20 (1), 38–56.

Luccioni, L. X., Pestana, J. M., Taylor, R. L., 2001. Finite element implementation of non-linear elastoplastic constitutive laws using local and global explicit algorithms with automatic error control. Int. J. Num. Meth. Engng. 50, 1191–1212.

Mašín, D., 2004. Laboratory and numerical modelling of natural clays. MPhil thesis. City University, London.

Mašín, D., 2005. A hypoplastic constitutive model for clays. Int. J. Num. Anal. Meth. Geomech. 29, 311–336.

Mašín, D., Chambon, R., Desrues, J., 2005. CLoE model modified to predict the behaviour of normally compressed clays. In: Proc. 11^{th} Int. Conference IACMAG. Turin, Italy.

Mašín, D., Herle, I., 2005. State boundary surface of a hypoplastic model for clays. Computers and Geotechnics 32 (6), 400–410.

Mroz, Z., Norris, V. A., Zienkiewicz, O. C., 1978. An anisotropic hardening model for soils and its application to cyclic loading. Int. J. Num. Anal. Meth. Geomech. 2, 203–221.

Niemunis, A., 2002. Extended hypoplastic models for soils. Habilitation thesis, Ruhr-University, Bochum.

Niemunis, A., Herle, I., 1997. Hypoplastic model for cohesionless soils with elastic strain range. Mech. Cohesive–Frictional Materials 2, 279–299.

Prevost, J. H., 1977. Mathematical modelling of monotonic and cyclic undrained clay behaviour. Int. J. Num. Anal. Meth. Geomech. 1, 195–216.

Rice, J. R., 1976. The localization of plastic deformations. In: Koiter (Ed.), Theoretical and Applied Mechanics. North–Holland.

Roscoe, K. H., Burland, J. B., 1968. On the generalised stress-strain behaviour of wet clay. In: Heyman, J., Leckie, F. A. (Eds.), Engineering Plasticity. Cambridge: Cambridge Univesrity Press.

Rouainia, M., Wood, D. M., 2001. Implicit numerical integration for a kinematic hardening soil plasticity model. Int. J. Num. Anal. Meth. Geomech. 25, 1305–1325.

Rudnicki, J. W., Rice, J. R., 1975. Conditions for the localization of deformation in pressure–sensitive dilatant materials. Journal of the Mechanics and Physics of Solids 23, 371–394.

Schofield, A. N., Wroth, C. P., 1968. Critical State Soil Mechanics. McGraw–Hill, London.

Smith, P. R., Jardine, R. J., Hight, D. W., 1992. The yielding of Bothkennar clay. Géotechnique 42 (2), 257–274.

St. John, H. D., Potts, D. M., Jardine, R. J., Higgins, K. G., 1993. Prediction and performance of ground response due to construction of a deep basement at 60 Victoria Embankment. In: Houlsby, G. T., Schofield, A. N. (Eds.), Predictive Soil Mechanics (Wroth Mem. Symp.). Thomas Telford, London.

Stallebrass, S. E., 1990. Modelling the effect of recent stress history on the behaviour of overconsolidated soils. Ph.D. thesis, The City University, London.

Stallebrass, S. E., Taylor, R. N., 1997. Prediction of ground movements in overconsolidated clay. Géotechnique 47 (2), 235–253.

Tamagnini, C., Viggiani, G., 2002. On the incremental non-linearity of soils. Part I: theoretical aspects. Rivista Italiana di Geotecnica 36 (1), 44–61.

Tamagnini, C., Viggiani, G., Chambon, R., 2000. A review of two different approaches to hypoplasticity. In: Kolymbas, D. (Ed.), Constitutive Modelling of Granular Materials. Springer, Berlin.

Tamagnini, C., Viggiani, G., Chambon, R., Desrues, J., 2002. Evaluation of different strategies for the integration of hypoplastic constitutive equations: Application to the cloe model. Mech. Cohesive–Frictional Materials 5, 263–289.

Truesdell, C. A., 1956. Hypo–elastic shear. J. Appl. Physics 27, 441–447.

van Eekelen, H. A. M., 1980. Isotropic yield surfaces in three dimensions for use in soil mechanics. Int. J. Num. Anal. Meth. Geomech. 4, 89–101.

Viggiani, G., Tamagnini, C., 2000. Ground movements around excavations in granular soils: a few remarks on the influence of the constitutive assumptions on FE predictions. Mech. Cohesive–Frictional Materials 5 (5), 399–423.

von Wolffersdorff, P. A., 1996. A hypoplastic relation for granular materials with a predefined limit state surface. Mech. Cohesive–Frictional Materials 1, 251–271.

Whittle, A. J., Hashash, Y. M. A., Whitman, R. V., 1993. Analysis of deep excavation in Boston. J. Geotech. Engng., ASCE 119 (1), 69–90.

Wood, D. M., 1974. Some aspects of the mechanical behavior of kaolin under truly triaxial conditions of stress and strain. Ph.D. thesis, Cambridge University.

Wu, W., Kolymbas, D., 2000. Hypoplasticity then and now. In: Kolymbas, D. (Ed.), Constitutive Modelling of Granular Materials. Springer, Berlin.

APPENDIX A

The results of all the stress–probing tests from the anisotropic initial state B, along with the corresponding predictions for the five models considered, are summarized in Figs. 15 ($q:\epsilon_s$ plane) and 16 ($p:\epsilon_v$ plane). Note that all strain measures are evaluated as natural strains.

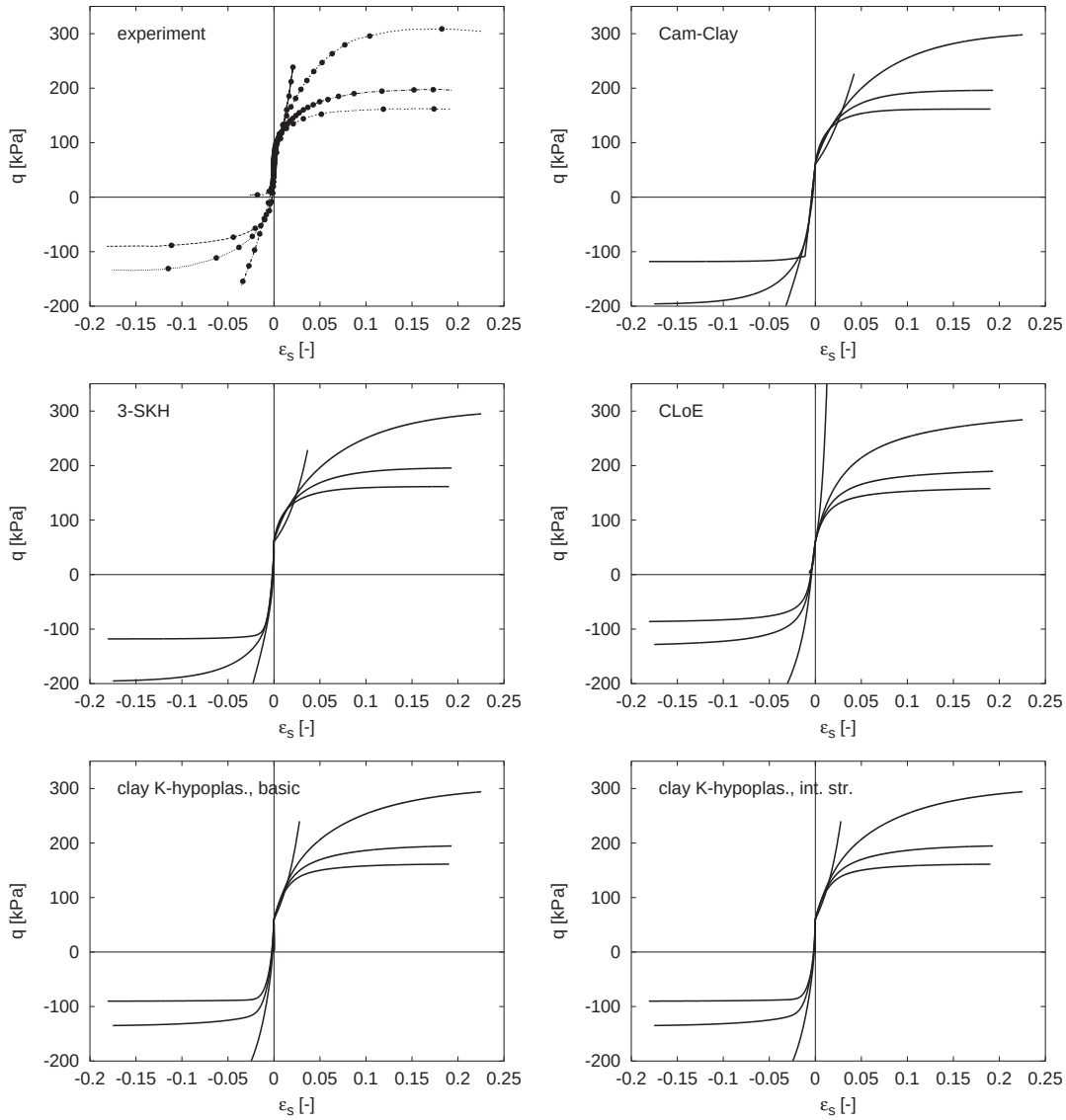

Figure 15. Experimental and predicted responses in the q:ϵ_s plane.

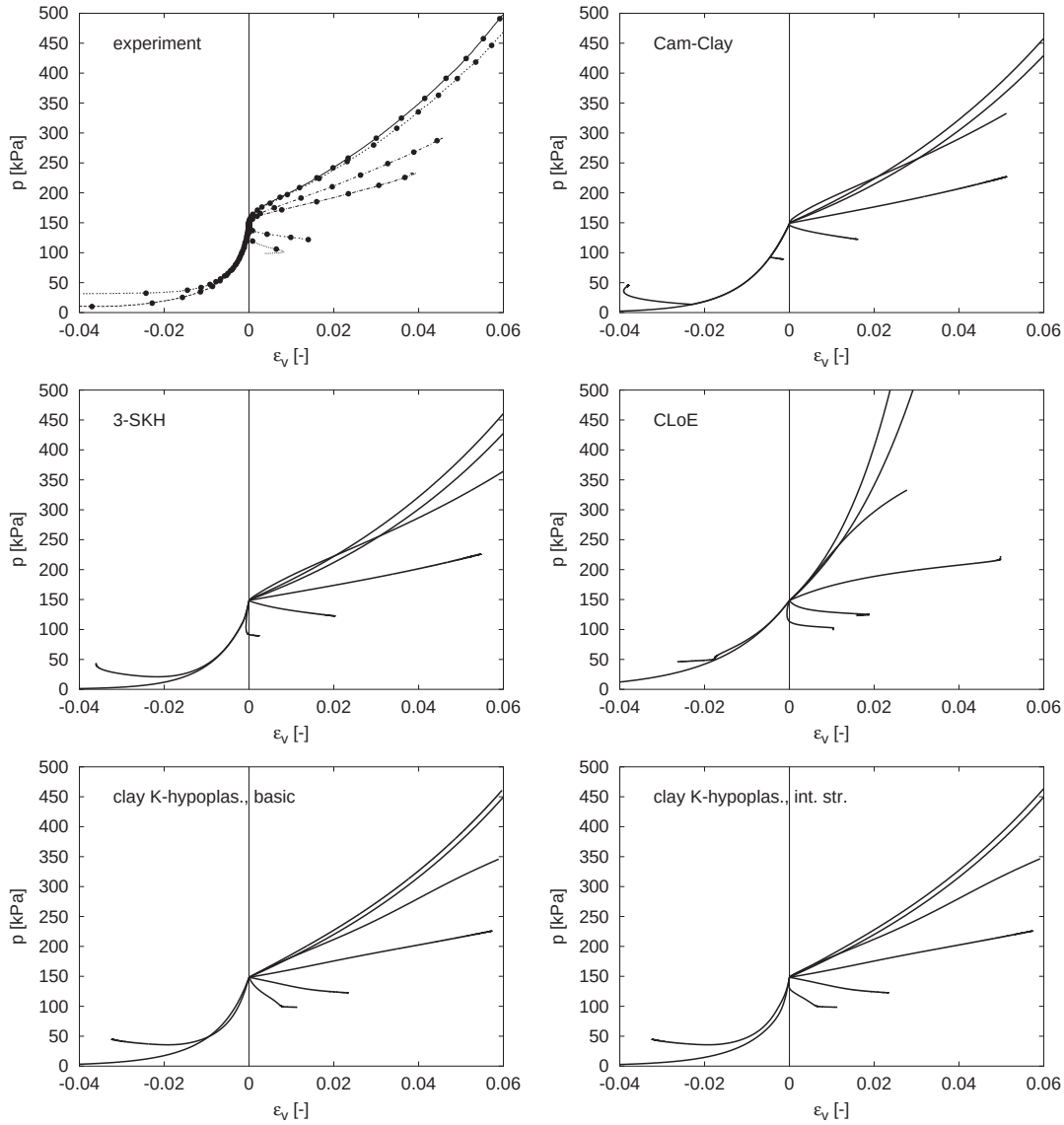

Figure 16. Experimental and predicted responses in the p:ϵ_v plane.

APPENDIX B: MATHEMATICAL FORMULATION OF THE CONSTITUTIVE MODELS

In the description of the relevant constitutive equations, the following invariant quantities for the stress tensor are used:

$$p := \frac{1}{3}\,\boldsymbol{\sigma} : \mathbf{1} \qquad q := \sqrt{\frac{3}{2}\boldsymbol{s} : \boldsymbol{s}} \qquad \cos(3\theta) := -\sqrt{6}\frac{\mathrm{tr}\left(\boldsymbol{s}^3\right)}{\left(\boldsymbol{s} : \boldsymbol{s}\right)^{3/2}} \tag{6.1}$$

where $\boldsymbol{s} = \boldsymbol{\sigma} - p\,\mathbf{1}$ is the deviatoric part of the stress tensor and $\mathbf{1}$ is the second–order identity tensor. Use is made of the fourth–order identity tensor $\boldsymbol{\mathcal{I}}$, with components:

$$\left(\boldsymbol{\mathcal{I}}\right)_{ijkl} := \frac{1}{2}\,\left(\delta_{ik}\delta_{jl} + \delta_{il}\delta_{jk}\right) \tag{6.2}$$

K–hypoplastic model for clays

The mathematical structure of the K–hypoplastic model for clays is discussed in detail in Mašín (2005). The constitutive equation in rate form reads:

$$\dot{\boldsymbol{\sigma}} = f_s \boldsymbol{\mathcal{L}} : \dot{\boldsymbol{\epsilon}} + f_s f_d \boldsymbol{N}\,\|\dot{\boldsymbol{\epsilon}}\| \tag{6.3}$$

where:

$$\boldsymbol{\mathcal{L}} := 3\left(c_1\boldsymbol{\mathcal{I}} + c_2 a^2 \hat{\boldsymbol{\sigma}} \otimes \hat{\boldsymbol{\sigma}}\right) \qquad \boldsymbol{N} = \boldsymbol{\mathcal{L}} : \left(Y\frac{\mathbf{m}}{\|\mathbf{m}\|}\right) \qquad \hat{\boldsymbol{\sigma}} := \frac{1}{3p}\,\boldsymbol{\sigma} \tag{6.4}$$

In eq. (6.3), the functions $f_s(p, e)$ (barotropy factor) and $f_d(e)$ (pyknotropy factor) are given by:

$$f_s = \frac{3p}{\lambda^*}\left(3 + a^2 - 2^\alpha a\sqrt{3}\right)^{-1} \qquad f_d = \left\{2p\,\exp\left[\frac{\ln\left(1+e\right) - N}{\lambda^*}\right]\right\}^\alpha \tag{6.5}$$

The scalar function Y and second–order tensor $\boldsymbol{m}$ appearing in eq. (6.4) are given, respectively, by:

$$Y = \left(\frac{\sqrt{3}a}{3+a^2} - 1\right)\frac{\left(I_1 I_2 + 9I_3\right)\left(1 - \sin^2\varphi_c\right)}{8I_3\sin^2\varphi_c} + \frac{\sqrt{3}a}{3+a^2} \tag{6.6}$$

in which:

$$I_1 := \mathrm{tr}(\boldsymbol{\sigma}) \qquad I_2 := \frac{1}{2}\left[\boldsymbol{\sigma} : \boldsymbol{\sigma} - (I_1)^2\right] \qquad I_3 = \det \boldsymbol{\sigma}$$

and:

$$\boldsymbol{m} = -\frac{a}{F}\left[\hat{\boldsymbol{\sigma}} + \mathrm{dev}\,\hat{\boldsymbol{\sigma}} - \frac{\hat{\boldsymbol{\sigma}}}{3}\left(\frac{6\hat{\boldsymbol{\sigma}} : \hat{\boldsymbol{\sigma}} - 1}{(F/a)^2 + \hat{\boldsymbol{\sigma}} : \hat{\boldsymbol{\sigma}}}\right)\right] \tag{6.7}$$

in which:

$$F = \sqrt{\frac{1}{8}\tan^2\psi + \frac{2 - \tan^2\psi}{2 + \sqrt{2}\tan\psi\cos 3\theta}} - \frac{1}{2\sqrt{2}}\tan\psi \qquad \tan\psi := \sqrt{3}\,\|\mathrm{dev}\,\hat{\boldsymbol{\sigma}}\| \tag{6.8}$$

Finally, the scalars a, α, c_1 and c_2 appearing in eqs. (6.4)–(6.7), are given as functions of the material parameters φ_c, λ^*, κ^* and r by the following relations:

$$a = \frac{\sqrt{3}\,(3 - \sin\varphi_c)}{2\sqrt{2}\sin\varphi_c} \qquad \alpha = \frac{1}{\ln 2}\,\ln\left[\frac{\lambda^* - \kappa^*}{\lambda^* + \kappa^*}\left(\frac{3 + a^2}{a\sqrt{3}}\right)\right] \tag{6.9}$$

$$c_1 = \frac{2\left(3 + a^2 - 2^\alpha a\sqrt{3}\right)}{9r} \qquad c_2 = 1 + (1 - c_1)\frac{3}{a^2} \tag{6.10}$$

The model requires five constitutive parameters, namely φ_c, λ^*, κ^*, N and r.

Integranular strain enhancement of K–hypoplasticity

As proposed by Niemunis and Herle (1997), the enhanced K–hypoplastic model is endowed with an additional state variable, $\boldsymbol{\delta}$, a second–order tensor defined as *intergranular strain*, which can be interpreted as a macroscopic manifestation of intergranular slips at grain contacts.

Let $\rho := \|\boldsymbol{\delta}\|/R$ be a suitable normalized magnitude of $\boldsymbol{\delta}$, R being a scalar model parameter. Also, let

$$\hat{\boldsymbol{\delta}} = \begin{cases} \boldsymbol{\delta}/\|\boldsymbol{\delta}\| & \text{for } \boldsymbol{\delta} \neq \mathbf{0} \\ \mathbf{0} & \text{for } \boldsymbol{\delta} = \mathbf{0} \end{cases} \tag{6.11}$$

denote intergranular strain direction. The constitutive equations for enhanced K–hypoplasticity for clays can be written as:

$$\dot{\boldsymbol{\sigma}} = \boldsymbol{\mathcal{M}} : \dot{\boldsymbol{\epsilon}} \tag{6.12}$$

where the fourth–order tangent stiffness tensor $\boldsymbol{\mathcal{M}}$ is calculated from the constitutive tensors tensors $\boldsymbol{\mathcal{L}}$ and $\boldsymbol{N}$ defined in eq. (6.4), the barotropy and pyknotropy factors given in eq. (6.5), and the intergranular strain tensor via the following interpolation:

$$\boldsymbol{\mathcal{M}} = \left[\rho^{\chi} m_T + (1 - \rho^{\chi})\, m_R\right] f_s \boldsymbol{\mathcal{L}} + \boldsymbol{\mathcal{B}} \tag{6.13}$$

where:

$$\boldsymbol{\mathcal{B}} := \begin{cases} \rho^{\chi}\,(1 - m_T)\, f_s \boldsymbol{\mathcal{L}} : \hat{\boldsymbol{\delta}} \otimes \hat{\boldsymbol{\delta}} + \rho^{\chi} f_s f_d \mathbf{N} \otimes \hat{\boldsymbol{\delta}} & (\hat{\boldsymbol{\delta}} : \dot{\boldsymbol{\epsilon}} > 0) \\ \rho^{\chi}\,(m_R - m_T)\, f_s \boldsymbol{\mathcal{L}} : \hat{\boldsymbol{\delta}} \otimes \hat{\boldsymbol{\delta}} & (\hat{\boldsymbol{\delta}} : \dot{\boldsymbol{\epsilon}} \leq 0) \end{cases} \tag{6.14}$$

and χ, m_T and m_R are material constants.

The evolution equation for the intergranular strain tensor $\boldsymbol{\delta}$ is given by

$$\dot{\boldsymbol{\delta}} = \begin{cases} \left(\boldsymbol{\mathcal{I}} - \hat{\boldsymbol{\delta}} \otimes \hat{\boldsymbol{\delta}} \rho^{\beta_r}\right) : \dot{\boldsymbol{\epsilon}} & (\hat{\boldsymbol{\delta}} : \dot{\boldsymbol{\epsilon}} > 0) \\ \dot{\boldsymbol{\epsilon}} & (\hat{\boldsymbol{\delta}} : \dot{\boldsymbol{\epsilon}} \leq 0) \end{cases} \tag{6.15}$$

As compared to the basic K–hypoplastic model for clay, the enhanced model requires five additional parameters, namely R, m_R, m_T, β_r and χ.

3-SKH model

The 3–SKH model is a nested–surface kinematic hardening plasticity model developed as an extension of classical Modified Cam–Clay. The original formulation is detailed in Stallebrass (1990). Herein, the version proposed by Stallebrass and Taylor (1997) is considered. The evolution equation for the effective stress tensor is given by:

$$\dot{\boldsymbol{\sigma}} = \boldsymbol{\mathcal{D}}^{e} : (\dot{\boldsymbol{\epsilon}} - \dot{\boldsymbol{\epsilon}}^{p}) \tag{6.16}$$

where $\dot{\boldsymbol{\epsilon}}$ is the plastic strain rate tensor and $\boldsymbol{\mathcal{D}}^e$ is the elastic tangent stiffness tensor, defined by:

$$\boldsymbol{\mathcal{D}}^e := \left(K - \frac{2}{3}G\right) \mathbf{1} \otimes \mathbf{1} + 2G\boldsymbol{\mathcal{I}} \qquad \frac{G}{p_r} = A\left(\frac{p}{p_r}\right)^n \left(\frac{p}{2a}\right)^m \qquad K = \frac{p}{\kappa^*}\,, \tag{6.17}$$

In the above equations, the scalar quantity a is an internal variable to be defined later, p_r is a reference stress (set equal to 1.0 kPa), and A, n and m are model parameters.

Nonlinearity and irreversibility are introduced by requiring the stress state to belong to the convex set (known as *elastic domain*):

$$\mathbb{E}_\sigma := \left\{ (\boldsymbol{\sigma}, a, \boldsymbol{\sigma}_b) \;\middle|\; f\left(\boldsymbol{\sigma}, a, \boldsymbol{\sigma}_b\right) \leq 0 \right\} \tag{6.18}$$

where $f(\boldsymbol{\sigma}, a, \boldsymbol{\sigma}_b)$ is the yield function of the material, given by:

$$f(\boldsymbol{\sigma}, a, \boldsymbol{\sigma}_b) = \frac{1}{2}\left[\left(\frac{\bar{q}_b}{M}\right)^2 + \bar{p}_b^2 - T^2 S^2 a^2\right] \tag{6.19}$$

In eq. (6.19), the scalar functions $\bar{p}_b$ and $\bar{q}_b$ are the first and second invariants of the tensor $(\boldsymbol{\sigma} - \boldsymbol{\sigma}_b)$, defined as in eq. (6.1); $\boldsymbol{\sigma}_b$ and a are internal variables, providing the coordinates of the centers of the yield surface and of the Bounding Surface (see eq. (6.21)), respectively, and M, T and S are model parameters.

Inside the yield surface, $\dot{\boldsymbol{\epsilon}}^p = \mathbf{0}$. For stress states on the yield surface, the plastic strain rate is given by the following associative flow rule:

$$\dot{\boldsymbol{\epsilon}}^p = \frac{\langle \boldsymbol{P} : \boldsymbol{\mathcal{D}}^e : \dot{\boldsymbol{\epsilon}} \rangle}{H + \boldsymbol{P} : \boldsymbol{\mathcal{D}}^e : \boldsymbol{P}}\, \boldsymbol{P} \qquad\qquad \boldsymbol{P} := \frac{\partial f}{\partial \boldsymbol{\sigma}} \tag{6.20}$$

where H is the plastic modulus and the operator $\langle x \rangle := (x + |x|)/2$ denotes the positive part of any scalar function x.

A key characteristic of the 3–SKH model is the definition of two additional surfaces in stress space. The first one, known as Bounding Surface, is given by:

$$F(\boldsymbol{\sigma}, a) = \frac{1}{2}\left[\left(\frac{q}{M}\right)^2 + p^2 - 2pa\right] \tag{6.21}$$

and limits the kinematic hardening of the yield surface. The second surface, called history surface, is given by:

$$f_h(\boldsymbol{\sigma}, a, \boldsymbol{\sigma}_a) = \frac{1}{2}\left[\left(\frac{\bar{q}_a}{M}\right)^2 + \bar{p}_a^2 - T^2 a^2\right] \tag{6.22}$$

where $\boldsymbol{\sigma}_a$ is an additional tensorial internal variable, and the scalar functions $\bar{p}_a$ and $\bar{q}_a$ are the first and second invariants of the tensor $(\boldsymbol{\sigma} - \boldsymbol{\sigma}_a)$.

The evolution equation for the scalar internal variable a is given by:

$$\dot{a} = \frac{a}{\lambda^* - \kappa^*}\, \dot{\boldsymbol{\epsilon}}^p : \mathbf{1} \tag{6.23}$$

where κ^* and λ^* are material constants. The kinematic hardening rules for the two back–stress tensors are given as follows:

1. *Plastic loading conditions with* $f_h < 0$ *and* $F < 0$

   In this case, we have:

$$\dot{\boldsymbol{\sigma}}_a = \frac{\dot{a}}{a}\boldsymbol{\sigma}_a \qquad\qquad \dot{\boldsymbol{\sigma}}_b = \frac{\dot{a}}{a}\boldsymbol{\sigma}_b + \dot{Z}_s\boldsymbol{\gamma} \tag{6.24}$$

   where:

$$\boldsymbol{\gamma} = \frac{\boldsymbol{\sigma} - \boldsymbol{\sigma}_b}{S} + \boldsymbol{\sigma}_a - \boldsymbol{\sigma} \tag{6.25}$$

$$\dot{Z}_s = \frac{1}{\boldsymbol{P} : \boldsymbol{\gamma}}\left\{\boldsymbol{P} : \left(\dot{\boldsymbol{\sigma}} - \frac{\dot{a}}{a}\,\boldsymbol{\sigma}_b\right) - T^2 S^2 a\dot{a}\right\} \tag{6.26}$$

2. *Plastic loading conditions with* $f_h = 0$ *and* $F < 0$

   In this case, we have:

$$\dot{\boldsymbol{\sigma}}_a = \frac{\dot{a}}{a}\boldsymbol{\sigma}_a + \dot{W}_s\boldsymbol{\beta} \tag{6.27}$$

   where:

$$\boldsymbol{\beta} = \frac{\boldsymbol{\sigma} - \boldsymbol{\sigma}_b}{TS} + a\,\mathbf{1} - \frac{\boldsymbol{\sigma} - \boldsymbol{\sigma}_b}{S} - \boldsymbol{\sigma}_a \tag{6.28}$$

$$\dot{W}_s = \frac{1}{\boldsymbol{P} : \boldsymbol{\beta}}\left\{\boldsymbol{P} : \left(\dot{\boldsymbol{\sigma}} - \frac{\dot{a}}{a}\,\boldsymbol{\sigma}_a\right) - T^2 S^3 a\dot{a}\right\} \tag{6.29}$$

The center of the yield surface, $\boldsymbol{\sigma}_b$ is now calculated explicitly from the non–intersection condition, as:

$$\boldsymbol{\sigma}_b = \boldsymbol{\sigma} - S(\boldsymbol{\sigma} - \boldsymbol{\sigma}_a) \tag{6.30}$$

3. *Plastic loading conditions with* $f_h = 0$ *and* $F = 0$

In this case, both back–stresses $\boldsymbol{\sigma}_a$ and $\boldsymbol{\sigma}_b$ can be obtained in closed form from the non–intersection condition, as:

$$\boldsymbol{\sigma}_a = \boldsymbol{\sigma} - T(\boldsymbol{\sigma} - a\,\mathbf{1}) \qquad\qquad \boldsymbol{\sigma}_b = \boldsymbol{\sigma} - TS(\boldsymbol{\sigma} - a\,\mathbf{1}) \tag{6.31}$$

The plastic modulus H is given by

$$H = h_0 + H_1 + H_2 \tag{6.32}$$

where:

$$h_0 = -\boldsymbol{P} : \left[\frac{\mathbf{1}}{\lambda^* - \kappa^*}\left(-T^2S^2a^2 - \boldsymbol{P} : \boldsymbol{\sigma}_b\right)\right] \tag{6.33}$$

$$H_1 = S^2\left(\frac{b_1}{b_{1\,\max}}\right)^{\psi}\frac{a^3}{\lambda^* - \kappa^*}\,; \qquad H_2 = \left(\frac{Tb_2}{b_{2\,\max}}\right)^{\psi}\frac{a^3}{\lambda^* - \kappa^*} \tag{6.34}$$

$$b_1 = \frac{\boldsymbol{\beta} : \boldsymbol{P}}{TSa}\,; \qquad b_2 = \frac{\boldsymbol{\gamma} : \boldsymbol{P}}{TSa} \tag{6.35}$$

$$b_{1\,\max} = 2a\,(1 - T)\;; \qquad b_{2\,\max} = 2Ta\,(1 - S) \tag{6.36}$$

The 3-SKH model requires 10 model parameters – namely λ^*, N^*, A, n, m, κ^*, M, T, S and ψ – and the definition of the initial conditions for 13 state variables, *i.e.*, the components of the tensors $\boldsymbol{\sigma}_a$ and $\boldsymbol{\sigma}_b$ and the scalar quantity a.